Energy 288 (2024) 129680

Contents lists available at ScienceDirect

Energy

journal homepage: www.elsevier.com/locate/energy

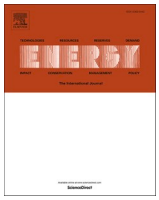

Risk-constrained stochastic scheduling for energy hub: Integrating renewables, demand response, and electric vehicles

Chengying Yang [a,b], Zhixin Wu [c,d,*], Xuetao Li [a,b], Ashk Fars [e]

[a] School of Economics and Management, Hubei University of Automotive Technology, Shiyan, 442000, Hubei, China
[b] Shiyan Industry Technique Academy of Chinese Academy of Engineering, Shiyan, 442000, Hubei, China
[c] College of Business Administration, Zhejiang University of Finance & Economics Dongfang College, Haining, 314408, Zhejiang, China
[d] College of Business Administration, Zhejiang University of Finance & Economics, Hangzhou, 310018, Zhejiang, China
[e] Automation and Engineering of Yerevn Company, Yerevan, Armenia

ARTICLE INFO

Handling Editor: X Ou

Keywords:
Risk-constrained stochastic scheduling
Energy hub management
Uncertainties
Slime mold algorithm
Coughing and chaos theory

ABSTRACT

This research introduces a stochastic scheduling approach that incorporates risk constraints for an energy hub (EH), considering uncertainties related to renewable generation and load demands. The proposed method utilizes the Conditional Value at Risk (CVaR) technique to assess and quantify risks. By striking a balance between reducing operational and emissions costs and increasing risk aversion, the approach presents a trade-off. The EH comprises various components such as a wind turbine (WT), photovoltaic (PV) cells, a fuel cell power plant (FCPP), a combined heat and power generation unit (CHP), and plug-in electric vehicles (PEVs). Uncertain variables encompass factors such as wind speed, solar irradiation, different demands, and market prices. To optimize profits and enhance the consumption curve, demand response programs (DRPs) for electrical, thermal, and cooling demands are implemented. To address the uncertainties associated with input random variables, the efficient k-means data clustering method is employed. A new slime mold algorithm, based on coughing and chaos theory, has been proposed to enhance the problem's solution. The algorithm incorporates innovative operators to improve its capabilities. By utilizing the coughing mechanism and chaos theory, the algorithm explores the solution space more effectively, resulting in improved outcomes for the problem at hand. The results demonstrate significant flexibility in EH management and are extensively discussed. Simulation results indicate that integrating PEVs, FCPP, and DRPs can lead to reductions of 2 %, 7 %, and 11 % in the EH's operating costs, respectively. Furthermore, considering PEVs, FCPP, and DRPs can improve the EH's risk cost by 1.98 %, 6.7 %, and 10.5 %, respectively. Based on the numerical results, in Case 4 led to a remarkable 12.65 % reduction in operational costs while simultaneously achieving a 15.43 % decrease in emission costs, showcasing the effectiveness of the proposed approach in optimizing energy management in an energy hub system.

1. Introduction

1-1. Difficulties and goals

The optimal management of energy hubs (EHs) presents significant difficulties and challenges due to the complex and dynamic nature of the system. Understanding and addressing these challenges is essential to achieve efficient and sustainable energy management [1]. Some of the key difficulties and goals in managing EHs include.

i) Nonlinear and Non-convex Optimization: The operation and control of EHs involve complex and nonlinear optimization problems. The interactions between different energy resources, storage systems, and loads create intricate relationships that require sophisticated optimization algorithms to find optimal solutions. Additionally, the non-convex nature of the problem further complicates the optimization process [2].
ii) Uncertainties in Renewable Generation and Load Demands: EHs heavily rely on renewable energy sources, which are inherently uncertain and variable [3]. Factors such as weather conditions, time of day, and seasonality can significantly affect the availability and output of renewable energy generation technologies. Moreover, load demands can also vary unpredictably, posing challenges in accurately forecasting and managing energy supply and demand [4].

* Corresponding author. College of Business Administration, Zhejiang University of Finance & Economics Dongfang College, Haining, 314408, Zhejiang, China.
E-mail address: 20150201@zufedfc.edu.cn (Z. Wu).

https://doi.org/10.1016/j.energy.2023.129680
Received 29 August 2023; Received in revised form 12 October 2023; Accepted 13 November 2023
Available online 17 November 2023
0360-5442/

Nomenclature

Abbreviation

MPPT	Maximum Power Point Tracking
PV	Photovoltaic
WT	Wind Turbine
FC	Fuel-Cell
HS	Hydrogen Storage
PEV	Plug-in electric vehicles

Indices

t	time
s	Scenario index
v	PEV index

Parameters and variables

PLR	Partial Load ratio
TER	Thermal energy ratio
P_{FC-Th}, P_{FC-El}	Thermal and electrical generation of fuel-cell
P_{FC}^{ch}	Electrical power required for hydrogen Production
P_{FC}^{disch}	Equivalent electrical power of consumed hydrogen
$P_{FC}^{min}, P_{FC}^{max}$	Minimum and maximum power contribution of FC
$P_{FC}^{ch,min}, P_{FC}^{ch,max}$	Minimum and maximum limit for charge power of FC
$P_{FC}^{disch,min}, P_{FC}^{disch,max}$	Minimum and maximum limit for discharge Power of FC
P_{H2}	Equivalent electrical power of stored hydrogen
η_{FC}	Efficiency of FC
$P_{H2}^{min}, P_{H2}^{max}$	Minimum and maximum limit of equivalent electrical power of hydrogen storage
$U_{H2}^{ch}, U_{H2}^{disch}$	Binary for hydrogen generation and hydrogen usage
η_{H2}	Efficiency of the hydrogen tank
A, B, C	WT power curve parameters
$W(t,s)$	Wind speed
$W^{cut,in}, W^{r}, W^{cut,out}$	Cut-in, rated and cut-out speeds for WT
P_{WT}, P_{WT}^{out}	Electrical power generated by WT
P_{WT}^{r}	Nominal power of WT
η_{WT}^{con}	WT converter efficiencies
P_{PV}, P_{PV}^{out}	Electrical power generated by PV
S	Solar radiation on PV panels
S^{std}	Solar radiation on PV panels at standard condition
T^{std}	Temperature of PV panels at standard condition
C_T	Temperature coefficient
N_{PV}^{pa}, N_{PV}^{se}	Number of solar parallel and series cells
T_{PV}	Temperature of PV panels
T_{Amb}	Ambient temperature
NOCT	Nominal operation cell temperature
η_{PV}^{con}	PV converter efficiencies
SOC	State of charge of PEV
P_{PEV}^{ch}, P_{PEV}^{disch}	Charge and discharge power of PEV
$\eta_{PEV}^{ch}, \eta_{PEV}^{disch}$	Efficiency of charge and discharge performance of PEV
P_{PEV-tr}	Power consumption of PEV during travel
SOC^{min}, SOC^{max}	Minimum and maximum limit for SOC of PEV
ΔD	Traveling distance of vth PEV
$P_{PEV}^{ch,min}$, $P_{PEV}^{ch,max}$	Minimum and maximum limit for charge power of PEV
$P_{PEV}^{disch}, P_{PEV}^{disch}$	Minimum and maximum limit for discharge power Of PEV
η_{PEV}	Efficiency of PEV
$U_{PEV}^{ch}, U_{PEV}^{disch}$	Binary for PEV charge and discharge performances
P_{Th-s}	Level of stored energy inside thermal storage
P_{Th-s}^{ch}	Charge power level of thermal storage
$Cost_{PV}, Cost_{WT}$	Cost of electricity generation with PV and WT
$Cost_{El-N}, Cost_{Th-N}, Cost_{G-N}$	Cost of power procurement from the electrical, thermal and gas markets
$Cost_{CHP}, Cost_{B}$	Cost of heat generation with CHP and boiler
$Cost_{Th-S}, Cost_{C-S}$	Operation cost of heating and cooling storages
$Cost_{El-DR}, Cost_{Th-DR}, Cost_{C-DR}$	Cost of electrical, thermal, and cooling DRP
$Cost_{UN-Em}, Cost_{CHP-Em}$	Cost of emissions with upstream network and CHP unit
$Cost_{B-Em}, Cost_{PC-Em}$	Cost of emissions with boiler and Fuel-cell
$\Psi_{El-N}, \Psi_{Th-N}, \Psi_{G-N}$	Electrical, thermal, and gas networks prices
Ψ_{Th-S}, Ψ_{C-S}	Price of operation for thermal and cooling storages
$\Psi_{El-Dr}, \Psi_{Th-Dr}, \Psi_{C-Dr}$	Price of participation in electrical, thermal, and cooling DRPs
P_{Th-s}^{disch}	Discharge power level of thermal storage
P_{Th-s}^{loss}	Power loss amount inside thermal storage
a_{Th-s}^{loss}	Factor for calculation of the thermal storage loss power
$\varphi_{Th-s}^{min}, \varphi_{Th-s}^{max}$	Factors for calculation of thermal storage minimum and maximum power level
P_{Th-s}^{Cap}	Nominal capacity of thermal storage
$\eta_{Th-s}^{ch}, \eta_{Th-s}^{disch}$	Efficiency of charge and discharge performance of thermal storage
$U_{Th-s}^{ch}, U_{Th-s}^{disch}$	Binary for thermal storage charge and discharge Performances
a_{C-S}^{loss}	Factors for calculation of cooling storage power
$\varphi_{Th-s}^{min}, \varphi_{Th-s}^{max}$	Factors for calculation of cooling minimum and power level
P_{C-S}^{cap}	Nominal capacity of cooling storage
$\eta_{Th-s}^{ch}, \eta_{Th-s}^{disch}$	Efficiency of charge and discharge performance of cooling storage
P_{C-S}	Level of stored energy inside cooling storage
P_{C-S}^{h}	Charge power level of cooling storage
P_{C-S}^{disch}	Discharge power level of cooling storage
P_{C-S}^{loss}	Power loss amount inside cooling storage
$U_{C-S}^{ch}, U_{C-S}^{ch}$	Binary for cooling storage charge and discharge performances
$P_{El}, P_{Th}, P_{C}, P_{G}$	Electrical, heating, cooling, and gas demands
$LPF_{El}^{shift,down}, LPF_{El}^{shift,up}$	Factors for decrement and increment of electrical load through DRP
$LPF_{Th}^{shift,down}, LPF_{Th}^{shift,up}$	Factors for decrement and increment of thermal load through DRP
$LPF_{C}^{shift,down}, LPF_{C}^{shift,up}$	Factors for decrement and increment of cooling load through DRP
$P_{El}^{shift,down}, P_{El}^{shift,up}$	Decreased and increased amount of electrical load with DRP
$U_{El}^{shift,down}, U_{El}^{shift,up}$	Binary for decreasing and increasing the electrical demand DRP
$P_{Th}^{shift,down}, P_{Th}^{shift,up}$	Decreased and increased amount of thermal load with DRP
$U_{Th}^{shift,down}, U_{Th}^{shift,up}$	Binary for decreasing and increasing thermal demand DRP
$P_{C}^{shift,down}, P_{C}^{shift,up}$	Decreased and increased amount of cooling load with DRP
$U_{C}^{shift,down}, U_{C}^{shift,up}$	Binary for decreasing and increasing the cooling demand thorough DRP
$P_{El-N}^{min}, P_{El-N}^{max}$	Minimum and maximum limit for power procurement from the electrical grid
$P_{G-N}^{min}, P_{G-N}^{max}$	Minimum and maximum limit for power procurement from gas network
$P_{Th-N}^{min}, P_{Th-N}^{max}$	Minimum and maximum limit for power procurement from thermal market
$\eta_{B}, \eta_{Tr}, \eta_{Chiller-El}, \eta_{Chiller-Ab}$	Efficiency of boiler, transformer,

electrical and absorption chiller

$\eta_{CHP-El}, \eta_{CHP-Th}$ Thermal and electrical productio efficiency of CHP

$P_B^{Cap}, P_{CHP}^{Cap}, P_{Tr}^{Cap}$ Nominal capacity of boiler, CHP and transformer

$P_{Chiller-El}^{Cap}, P_{Chiller-Ac}^{Cap}$ Nominal capacity of electrical and absorption Chiller

$P_{El-N}^{Cap}, P_{Tr-N}^{Cap}, P_{G-N}^{Cap}$ Amount of energy procurement from electrical, thermal, and gas networks

P_B Gas power received by boiler

P_{CHP} Gas power received by CHP

$P_{Chiller-El}$ Electrical power received by electrical Chiller

$P_{Chiller-Ab}$ Thermal power received by absorption Chiller

Ψ_{Em} Price of green gas emissions

Ψ_{WT}, Ψ_{PV} Price of WT and PV production

$\Psi_{H2-Pump}$ Price of WT and PV production

$Em_{El-CO2}, Em_{El-NOx}, Em_{El-SO2}$ Factors for electrical network CO2, NOx, and SO2 emissions

$Em_{CHP-CO2}, Em_{CHP-NOx}, Em_{CHP-SO2}$ Factors for CHP CO2, NOx and SO2 emissions

$Em_{B-CO2}, Em_{B-NOx}, Em_{B-SO2}$ Factors for fuel-cell CO2, NOx and SO2 emissions

$Em_{FC-CO2}, Em_{FC-NOx}, Em_{FC-SO2}$ Factors for boiler CO2, NOx and SO2 emissions

$\Psi_{CO2}, \Psi_{NOx}, \Psi_{SO2}$ Price for the emission of CO2, NOx, and SO2 gases

P_S Probability of each scenario

iii) Efficient Resource Integration: EHs aim to integrate diverse energy resources, including renewable energy generation technologies, energy storage systems, and flexible loads. Efficiently coordinating the operation of these resources is critical to ensure optimal energy production, consumption, and distribution. However, achieving this integration and balancing the energy flow across different components can be technically challenging [5].

iv) Risk and Uncertainty Management: The uncertainties associated with renewable generation and load demands introduce risks in EH operation and planning. It is crucial to develop robust strategies that can account for and mitigate these risks effectively [6]. This includes incorporating risk assessment and management techniques to make informed decisions and ensure the reliability and resilience of EHs [7].

The overarching goal in managing EHs is to achieve optimal utilization of diverse energy resources while meeting energy demands, reducing environmental impact, and ensuring economic viability. This involves developing advanced modeling and optimization methods that consider the complexities and uncertainties inherent in EHs. By addressing these difficulties and goals, EHs can play a significant role in advancing the transition towards a sustainable and low-carbon energy future [8].

1-2. Litrature review

A significant amount of research has been dedicated to addressing the challenges and opportunities associated with the effective management of energy hubs (EHs) [9]. These research efforts have spanned various domains, encompassing the development of models and optimization methods, the integration of renewable energy sources, the implementation of demand response initiatives, and the formulation of strategies for risk management. One pivotal area of research in EH management revolves around the creation of mathematical models and optimization algorithms. Researchers have explored diverse mathematical frameworks, including mixed-integer linear programming (MILP), mixed-integer nonlinear programming (MINLP), and stochastic programming, to capture the intricacies and nonlinearity of EH operations [10]. These models are designed to identify optimal scheduling and dispatch strategies that minimize operational costs, emissions, or a combination of economic and environmental objectives. Advanced optimization techniques, such as evolutionary algorithms, particle swarm optimization, and genetic algorithms, have also been employed to tackle the non-convex nature of EH optimization problems [11]. The integration of renewable energy sources into EHs has been a focal point of research. Studies have delved into effective methods for incorporating wind turbines, photovoltaic cells, and other renewable generation technologies into the EH infrastructure [12]. Techniques like forecasting, predictive control, and real-time optimization have been explored to better manage the variability and uncertainty associated with renewable energy generation. Energy storage systems, such as batteries and pumped hydro storage, have also been investigated to enhance the flexibility and reliability of EHs by storing excess energy during periods of high generation and supplying it during periods of high demand [13–15]. Demand response programs (DRPs) have been acknowledged as valuable tools in EH management. DRPs involve adjusting energy consumption patterns based on price signals, grid conditions, or other incentives to optimize energy use and reduce peak demand [16]. Researchers have proposed various strategies, such as load shifting, demand-side management, and smart grid technologies, to enable effective demand response in EHs [17]. These programs can not only improve the EH's operational efficiency but also contribute to grid stability and reduce overall energy costs [18]. Risk management and uncertainty handling have also garnered significant attention in EH literature [19]. Researchers have explored techniques such as robust optimization, stochastic programming, and scenario-based approaches to address the uncertainties associated with renewable energy generation and load demands [20]. Risk assessment methods, including conditional value at risk (CVaR), probability distribution functions, and Monte Carlo simulation, have been employed to quantify and manage the risks involved in EH operations [21–23]. By explicitly considering uncertainties, these studies aim to enhance the decision-making process and bolster the resilience of EHs against unexpected events [24]. In a research study conducted by Ref. [25], a stochastic scheduling method was introduced, utilizing Conditional Value at Risk (CVaR) for the operational management of an Energy Hub (EH). This strategy considered uncertainties in electricity and natural gas prices, along with electricity usage patterns. The optimization framework integrated factors such as operational efficiency, emissions, and potential risks to enhance the overall performance of the EH. In a different research effort [26], the focus was on collectively managing the energy usage of multiple EHs to minimize overall operational costs. This analysis integrated Demand Response (DR) initiatives that adjusted both electrical and thermal loads to achieve the best possible energy consumption outcomes. In Ref. [27], a two-level method was proposed to coordinate the operation of a distribution network and interconnected EHs. The higher-level optimization aimed at reducing operational expenses in the distribution network, while the lower-level optimization aimed to cut down the total operational costs of the EHs. In Ref. [28], the optimal scheduling of an energy hub was explored, encompassing electrical, thermal, and water requirements. The primary objective of this optimization challenge was to reduce operational expenses in the energy system while ensuring efficient water extraction for future needs. The research employed an epsilon constraint approach and a fuzzy satisfying strategy to identify the most advantageous payoff options. Additionally [29], focused on the optimal operation of an Energy Hub (EH) using fuel-cell/Combined Heat and Power (CHP) technology, taking into account the existence of Demand Response Programs (DRPs) for both electrical and thermal aspects. In Ref. [30] introduced a risk-averse

multi-objective approach aimed at addressing the self-scheduling challenges of virtual energy hub plants. The virtual energy hub plant in question operates across various energy carriers, including electricity, heating, cooling, and hydrogen, incorporating P2X units, electric vehicles, and an innovative demand response (DR) strategy. In Ref. [31] explored the optimal operation of a distribution network that incorporates renewable resources and a novel liquid carbon dioxide energy storage system. It introduces a comprehensive modeling and optimization framework for integrating wind turbines and solar sources with the innovative energy storage system, taking into account their respective converters. In Ref. [32] introduced a day-ahead scheduling framework for energy hubs (EH) operating in energy and reserve markets, with a focus on optimizing both economic and environmental objectives. The EH under examination comprises a unique hybrid energy storage system incorporating a fuel cell, wind power, photovoltaic energy, and a specialized fuel cell unit, all within the context of elastic demand. Table 1 presents a comparison of the referenced studies based on their advantages and disadvantages.

The objective of the study was to optimize the EH's performance while effectively managing risks. Overall, these studies highlight various approaches to optimize the operation of EHs, considering factors such as uncertainties, DR programs, coordinated management, and risk assessment. By employing advanced optimization techniques and considering multiple factors, these studies contribute to the efficient and effective operation of EHs.

1-3. Contributions and novelties

The literature review provides an extensive overview of various approaches used to optimize the operation of Energy Hubs (EHs), taking into account factors such as uncertainties, demand response programs, coordinated management, and risk assessment. These studies employ advanced optimization techniques and consider multiple variables to contribute to the efficient and effective operation of EHs. However, there exists a scientific gap in the current research landscape, particularly concerning risk-constrained stochastic scheduling approaches that address uncertainties in renewable generation and load demands. To address this gap, the proposed slime mold algorithm, based on coughing and chaos theory, is introduced as a novel solution to enhance the solution quality of EH management problems. The incorporation of this algorithm is expected to improve the flexibility of EH management and result in significant cost reductions. The outcomes and implications of this research are thoroughly discussed, highlighting the potential benefits of integrating plug-in electric vehicles (PEVs), fuel cell power plants (FCPP), and demand response programs (DRPs) into EHs. The research's key highlights and innovations are summarized as follows.

i) Risk-Constrained Stochastic Scheduling: The study introduces a novel approach for scheduling energy hubs (EHs) that incorporates risk considerations. By employing the conditional value at risk (CVaR) technique, the proposed approach assesses and manages the uncertainties associated with renewable generation and load demands.
ii) Balancing Costs and Risk Aversion: The research addresses the tradeoff between reducing operation and emissions costs while increasing risk aversion. The optimization framework aims to find a balance that maximizes the EH's performance by considering the costs and risks associated with different energy resources and demand response programs.
iii) The Energy Hub (EH) incorporates an assortment of energy sources, such as a wind turbine, solar panels, a fuel cell power plant, a combined heat and power generation unit, and electric vehicles. Through the integration of these diverse resources, the EH can effectively oversee the generation, utilization, and distribution of energy.
iv) Demand Response Programs (DRPs): To optimize profit and improve the consumption curve, the study implements DRPs for electrical, thermal, and cooling demands. These programs enable the EH to adjust energy consumption patterns based on price signals or other incentives, contributing to operational efficiency and cost reduction.
v) Innovative Solution Algorithm: The research proposes a new slime mold algorithm based on coughing and chaos theory to enhance the solution of the EH management problem. The algorithm incorporates innovative operators that effectively explore the solution space, leading to improved outcomes and more efficient EH management.
vi) Uncertainty Management: The study addresses the uncertainties associated with renewable generation and load demands, which are inherent in EH operations. This method is employed to manage uncertainties in input random variables, allowing for more robust and informed decision-making.

Table 1
Summary of benefits and drawbacks of referenced studies on energy hub management.

Paper Title	Focus	Key Disadvantages
Paper [9]	EH Models & Optimization Methods	Lack of consideration for uncertainty
Paper [10]	Mathematical Models & Optimization Algorithms	Limited exploration of advanced optimization techniques
Paper [12]	Integration of Renewable Energy Sources	Potential issues related to managing variability
Paper [16]	Demand Response Programs (DRPs)	Complexity of EH operations
Paper [19]	Risk Management & Uncertainty Handling	Potential complexity in implementing risk assessment
Paper [25]	Stochastic Scheduling & CVaR	Uncertainties in prices and usage patterns not fully addressed
Paper [26]	Multi-EH Management & DR Initiatives	No specific disadvantages mentioned
Paper [27]	Coordination of Distribution Network & EHs	Potential challenges in coordination
Paper [28]	Optimal Scheduling of EHs	Use of epsilon constraint approach may have limitations
Paper [29]	EH with Fuel-Cell/CHP & DRPs	Potential challenges in optimizing dual aspects
Paper [30]	Risk-Averse Multi-Objective Approach	Complex multi-objective optimization may require extensive computation
Paper [31]	Distribution Network with CO2 Energy Storage	New storage technology may pose integration challenges
Paper [32]	Day-Ahead Scheduling of EHs	Specific disadvantages not mentioned

1-4. Paper layout

The article can be continued in the following sections. The second part discusses problem modeling and objective functions. In the third part, the proposed developed algorithm is presented. The fourth part focuses on the results of simulation and numerical analysis. Finally, the fifth section presents the conclusions and suggestions for further work.

2. Problem formulation and objective functions

In this section, the mathematical modeling is described. To enhance clarity and organization, each concept and model utilized in the planning process is discussed separately in dedicated sections.

2-1. Fuel cell power plant

In Fig. 1, the schematic structure of the Fuel-cell power plant is depicted, featuring a Fuel Cell (FC), a reformer for thermal energy recovery, and a heat recovery system. Supporting components include a power conditioning unit, control system, hydrogen storage, and

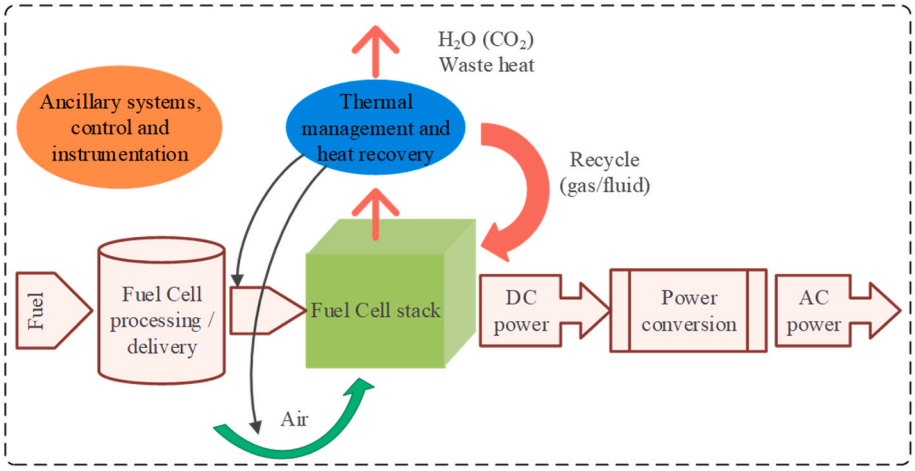

Fig. 1. Illustrates the schematic structure of the Fuel-cell power plant.

auxiliary systems for efficient electricity generation. Given the circumstances provided, it is possible to evaluate the thermal energy generated by the Fuel Cell (FC). Furthermore, the thermal energy produced by the FC can be captured at elevated temperatures within the reformer to enhance the overall efficiency of the Fuel Cell Power Plant (FCPP). The calculation of thermal power takes into account Thermal Energy Recovery (TER) [33]. Conversely, the efficiency of the FC depends on the electrical power it generates. The efficiency equations of the FC and TER can be described as follows:

$$if\ PLR < 0.05 \Rightarrow \begin{cases} \eta_{FC} = 0.2716 \\ TER = 0.6801 \end{cases} \tag{1}$$

$$if\ PLR > 0.05 \Rightarrow \begin{cases} \eta_{FC} = 0.9033 \times PLR^5 - 2.9996 \times PLR^4 + 3.6505 \times PLR^3 - 2.0704 \times PLR^2 + 0.4623 \times PLR + 0,3747 \\ TER = 1.0785 \times PLR^5 - 1.9739 + 1.5005 \times PLR^5 - 1.9739 + 1.5005 \times PLR^2 - 0.2817 \times PLR + 0.6838 \end{cases} \tag{2}$$

The relationship between the recovered thermal power and TER is denoted by Equation (3). Additionally, the operational boundaries of the FC are expressed through minimum and maximum limits, as stated in Equation (4):

$$P_{FC-TH(T,S)} = TER_{(T,S)} \times \left[P_{FC-EL(T,S)} + P_{FC}^{ch}(t.s)\right] \tag{3}$$

$$P_{FC}^{min} \le P_{FC-El}(t,s) + P_{FC}^{ch}(t,s) \le P_{FC}^{max}(t,s) \le P_{FC}^{max} \tag{4}$$

Surplus electrical power generated by the Fuel Cell Power Plant (FCPP) beyond its maximum capacity is utilized for hydrogen production. The equation establishes the relationship between recovered thermal power and TER while also defining the operational limits of the fuel cell (FC) within a specified range. The primary flow from the reformer contributes to the generation of both electrical and thermal power, while the supplementary flow is dedicated solely to the production of electrical power. Any excess hydrogen produced is stored in a hydrogen tank for future use. The provided equation enables the calculation of the corresponding electrical power derived from the stored hydrogen. It's essential to note that the capacity of the hydrogen tank is limited, necessitating the imposition of constraints on the equivalent electric power within specified lower and upper thresholds. The charging and discharging actions of hydrogen adhere to the technical restrictions outlined in the equations:

$$P_{FC}^{ch,min} \times U_{H_2}^{ch}(t,s) \le P_{FC}^{ch}(t,s) \le P_{FC}^{ch,max} \times U_{H_2}^{ch}(t,s) \tag{5}$$

$$P_{FC}^{disch,min} \times U_{FC}^{disch}(t,s) \le P_{FC}^{disch}(t,s) \le P_{FC}^{disch,max} \times U_{H_2}^{disch}(t,s) \tag{6}$$

$$U_{H_2}^{ch}(t,s) + U_{H_2}^{disch} = 1 \tag{7}$$

In each scenario and time period, only either charging or discharging is considered suitable for hydrogen storage.

2-2. Solar panel modeling

The performance of solar modules relies on various factors, including sunlight, temperature, humidity, and battery charge status. In this case study, a highly accurate mathematical model is employed to calculate the electric power output of solar modules, as demonstrated in Ref. [34]:

$$p_{pv}(t) = \eta_{pvg} \times A_{pvg} \times G(t) \tag{8}$$

This equation incorporates the instantaneous solar radiation (G(t), KW/m^2), the module area (A_{pvg}, m^2), and η_{pvg} the overall efficiency of the solar system, derived from:

$$\eta_{pvg} = \eta_{pv} \times \eta_{rec}\left[1 - \beta\left(T_c(t) - T_{c,ref}\right)\right] \tag{9}$$

Additionally, η_{pv} the solar module efficiency corresponds to the charge efficiency (η_{rec}) of the controller, equivalent to the MPPT inverter-charger ($\eta_{rec} = 1$). The temperature coefficient (TC) for the specific module is determined by the reference temperature ($T_{c,ref}$) of solar cells and calculated using:

$$T_c(t) = T_a(t) + \left(\frac{NOCT - 20}{800}\right) \times G_t \tag{10}$$

where, *NOCT* the normal operating temperature of the cell is the ambient air temperature ($T_a(t)$) at any moment. Finally, the total output power of solar modules is calculated from $P_{pv}(t) = N_{pv} \times p_{pv}(t)$ which N_{pv} is the total number of solar modules.

2-3. Wind turbine

The electricity generation of a wind turbine (WT) is described by an

equation that takes into account the nominal power, wind speed, and generated parameters [34]:

$$P_{WT}(W(t,s)) = \left\{ P^{r}_{wr} \times \left[C - BW^{0}_{P^{r}_{wr}}(t,s) + AW(t,s)^{2} \right] \right. \tag{11}$$

$$W(t,s) \le W^{cut,in} \& W(t,s) \ge W^{cut,out} \tag{12}$$

$$W^{cut.in} \le W(t,s) \le W^{r} \tag{13}$$

$$W^{r} \le W(t,s) \le W^{cut,out} \tag{14}$$

where W (t, s) represents the wind speed, and the generation is limited by cut-in and cut-out wind speed thresholds. The WT's power generation is modeled based on its power curve. The power generation of the Wind Turbine (WT) adheres to a predetermined curve determined by its power characteristics. In order to prioritize safety, the WT does not generate power when wind speeds fall below the cut-in threshold or exceed the cut-out threshold. Within the valid range of wind speeds, the WT produces power at its rated capacity.

2-4. Plug-in vehicles

Plug-in vehicles encompass electric vehicles (EVs) that can be charged from an external power source, usually an electrical grid. This category includes both plug-in hybrid electric vehicles (PHEVs) and battery electric vehicles (BEVs). PHEVs are equipped with an electric motor and an internal combustion engine, enabling them to switch between electric and gasoline power sources, whereas BEVs are entirely electric and depend solely on their electric motors for propulsion. Plug-in vehicles offer the benefit of decreased emissions and reduced reliance on fossil fuels, making them a more sustainable and environmentally friendly transportation choice. Owever, there are certain limitations to the operation of PEVs. These limitations may include factors such as limited driving range, longer charging times compared to refueling conventional vehicles, availability of charging infrastructure, and potential constraints on the overall electricity grid capacity for widespread PEV adoption [35]:

$$SOC(t,s,v) = SOC(t-1,s,v) + \eta^{ch}_{PEV}(v) \times P^{ch}_{PEV}(t_0,s,v) - \frac{P^{disch}_{PEV}(v)}{\eta^{disch}_{PEV}(v)} - P^{tr}_{PEV}(t_0,s,v) \tag{15}$$

$$SOC^{min} \le SOC(t,s,v) \le SOC^{max} \tag{16}$$

$$P_{PEV-tr}(t,s,v) = \Delta D(t,s,v) \times \eta_{PEV}(v) \tag{17}$$

$$P^{ch,min}_{PEV} \times U^{ch}_{PEV}(t,s,v) \le P^{ch}_{PEV}(t,s,v) \le P^{ch,max}_{PEV} \times U^{ch}_{PEV}(t,s,v) \tag{18}$$

$$P^{disch}_{min} \times U^{disch}_{PEV}(t,s,v) \le P^{disch,max}_{PEV} \times U^{disch}_{PEV}(t,s,v) \tag{19}$$

$$0 \le U^{sch}_{PEV}(t,s,v) + U^{disch}_{PEV}(t,s,v) \le 1 \tag{20}$$

The current level of stored electrical energy in the fifth Plug-in Electric Vehicle (PEV) is determined using Equation (15). Each PEV's State of Charge (SOC) is constrained within predefined minimum and maximum limits, as indicated by Equation (16). PEVs operate in three distinct modes: charge mode, discharge mode, and travel mode. The power consumption during the travel mode of PEVs is modeled by Equation (17). The permissible rates for charging and discharging each PEV are specified in Equation (19). Furthermore, the operation of PEVs is limited to a single scenario within each time period, and the concurrent operation of the cooling storage device in both modes prevents charging and discharging activities.

2-5. Thermal storage system

A typical thermal storage system comprises a storage medium, which can be substances such as water, ice, molten salt, or specialized materials stored in dedicated tanks. This storage medium collects energy during specific periods and subsequently releases it during different times. The process of modeling thermal storage is explained in the provided equations. One of the equations defines the current quantity of thermal energy held within the storage apparatus. This quantity determines the charging and discharging power rates, the speed of energy dissipation, and the amount of thermal energy stored in the preceding period. The method for calculating the energy loss rate within the storage system can be derived using the approach elucidated in Ref. [36].

$$P_{Th} - s(t,s) = P_{Th} - s(t-1,s) + P^{ch}_{Th-S}(t,s) - P^{disch}_{Th-S}(t-s) \tag{21}$$

$$P^{loss}_{Th-S}(t,s) = \alpha^{loss}_{Th-S} \times P_{Th-S}(t,s) \tag{22}$$

The power capacity of the thermal storage system is limited by the manufacturer based on factors like the volume of the storage material in the tanks and its current charging and discharging status. This constraint is further explained in the equation provided:

$$\varphi^{min}_{C-S} \times P^{cap}_{C-S} \leqslant P_{C-S}(t,s) \leqslant \varphi^{max}_{C-S} \times P^{cap}_{C-S} \tag{23}$$

$$\frac{\varphi^{\min}_{C-S} \times P^{cap}_{C-S}}{\eta^{ch}_{C-S}} \times U^{ch}_{C-S}(t,s) \le P^{ch}_{C-S}(t,s) \le \frac{\varphi^{\max}_{C-S} \times P^{cap}_{C-S}}{\eta^{ch}_{C-S}} \times U^{ch}_{C-S}(t,s) \tag{24}$$

$$\varphi^{\min}_{C-S} \times P^{cap}_{C-S} \times \eta^{disch}_{C-S} \times U^{disch}_{C-S}(t,s) \le P^{disch}_{C-S}(t,s) \le \varphi^{\max}_{C-S} \times P^{\max}_{C-S} \times \eta^{disch}_{C-S} \times U^{disch}_{C-S}(t,s) \tag{25}$$

In each period and scenario, the operation mode of the storage system is restricted to either charging or discharging, but not both simultaneously:

$$U^{ch}_{Th-S}(t,s) + U^{disch}_{Th-S}(t,s) = 1$$

2-6. Cooling storage system

In the proposed energy hub, a cooling storage system is seamlessly integrated to enhance the overall efficiency and functionality of the hub. The cooling storage system is designed to store excess cooling capacity during periods of low demand or high renewable energy generation. This stored cooling capacity can then be utilized during peak demand periods or when renewable energy generation is limited. By effectively managing the cooling storage, the energy hub can optimize its cooling resources, reduce energy waste, and provide reliable cooling services to meet the varying needs of the users. The integration of cooling storage contributes to a more sustainable and efficient operation of the energy hub [5]:

$$P_{C-S}(t,s) = P_{C-S}(t-1,s) + P^{ch}_{C-S}(t,s) - P^{disch}_{C-S}(t,s) - P^{loss}_{C-S}(t,s)$$

$$P^{loss}_{C-S}(t,s) = \alpha^{loss}_{C-S} \times P_{C-S}(t,s)$$

To account for the specific technology used in the construction of the cooling storage system, additional constraints are incorporated to address design parameters associated with the storage system. These parameters encompass elements such as pump sizes, compressor sizes, or specialized tanks tailored for the storage of the cooling material. These considerations are taken into consideration to guarantee appropriate sizing and efficient operation of the cooling storage within the broader framework of the energy hub:

$$\varphi^{min}_{C-S} \times P^{cap}_{C-S} \leqslant P_{C-S}(t,s) \leqslant \varphi^{max}_{C-S} \times P^{cap}_{C-S} \tag{26}$$

$$\frac{\varphi^{\min}_{C-S} \times P^{cap}_{C-S}}{\eta^{ch}_{C-S}} \times U^{ch}_{C-S}(t,s) \le P^{ch}_{C-S}(t,s) \le \frac{\varphi^{\max}_{C-S} \times P^{cap}_{C-S}}{\eta^{ch}_{C-S}} \times U^{ch}_{C-S}(t,s) \tag{27}$$

$$\varphi^{\min}_{C-S} \times P^{cap}_{C-S} \times \eta^{disch}_{C-S} \times U^{disch}_{C-S}(t,s) \le P^{disch}_{C-S}(t,s) \le \varphi^{\max}_{C-S} \times P^{\max}_{C-S} \times \eta^{disch}_{C-S} \times U^{disch}_{C-S}(t,s) \tag{28}$$

In each period and scenario, the operation mode of the storage system is limited to either charging or discharging mode, but not both simultaneously:

$$U_{C-S}^{ch}(t,s) + U_{C-S}^{disch}(t,s) = 1 \tag{29}$$

2-7. Network security

This research paper incorporates network enhancement by integrating Battery Energy Storage Systems (BESS), diesel generators, and a flexible charging strategy to optimize the cost of the enhancement. The maximum capacity of each line is determined by equation (30), which is calculated by multiplying the base capacity with an amplification factor. The amplification factor, considered as a design variable, is determined during the planning phase [37]:

$$\left|p_L^{s.i.vn.ts.td}\right| \le p_{max}^{i.j} \times L_r^{i.j} \forall s \in S.i \in N_{cs}.ts \in TS.td \in TD \tag{30}$$

2-8. Demand-side management

Demand-side management involves modeling load curve results by considering Demand Response Programs (DRP) and utilizing formula (31). Additionally, the limits for increasing and decreasing demand are applied through formulas (32) and (33) respectively. Formula (34) indicates that the increase and decrease in demand on a given day are equal. Furthermore, the restriction of not using simultaneous increases and decreases in demand more than once in a period is enforced by formula (35) [38]:

$$P_t^{el,DRP} = P_t^{el} + P_t^{shup,e} - P_t^{shdo,e} \tag{31}$$

$$0 \le P_t^{shup,e} \le LPF^{shup,e} \times P_t^{l} \times I_t^{shup} \tag{32}$$

$$0 \le P_t^{shdo,e} \le LPF^{shdo,e} \times P_t^{l} \times I_t^{shdo} \tag{33}$$

$$\sum_t^H P_t^{shup,e} = \sum_t^H P_t^{shdo,e} \tag{34}$$

$$I_t^{shup,e} + I_t^{shdo,e} \le 1 \tag{35}$$

2-9. Risk assessment

The existence of uncertainties in the input variables requires an elevation in risk mitigation measures. The Energy Hub (EH) is employed to effectively handle the potential risks linked to encountering significant fluctuations in the timing and cost of infrastructure release. Specifically, the Conditional Value at Risk (CVaR) infrastructure release [39] is utilized within the EH framework to address and manage such risks:

$$Min\ VAR + \frac{1}{1-\alpha}\sum_s p_s \lambda_s \tag{36}$$

$$\lambda_s \ge 0 \tag{37}$$

$$Cost_s - VAR \leqslant \lambda_s \tag{38}$$

Equation (36) introduces the concept of VAR (Value at Risk), where the term "Costs" refers to the cumulative expenses associated with scheduling and emissions within the energy hub for the s-th scenario, while the parameter α denotes the chosen level of confidence. Equations (37) and (38) utilize the auxiliary variable λs for risk calculation. If VAR exceeds Costs, λs is set to zero, while if Costs exceed VAR, λs is the difference between Costs and VAR.

2-10. Objective function

The objective function is designed to optimize the operation of the energy hub by considering the scheduling cost (EH CostSch), emission cost (CostEm), and risk cost (CostR). The weighting factor β is employed to establish a balance or compromise between minimizing the overall anticipated planning cost, emission cost, and risk. It allows for the consideration of various factors and their relative importance in the decision-making process. The scheduling cost includes expenses related to power exchange, demand response programs, and the operation of various energy hub components such as CHP, boiler, PV, WT, FCPP, and energy storage devices. The emission cost takes into account the environmental impact of the upstream network and energy hub components like CHP, boiler, and FCPP:

$$\text{O.f.} = \sum_{t=1}^{24}\sum_{s=1}^{10}(1-\beta)P_S[\cos ts_h + \cos te_m] + \beta[\cos tr] \tag{39}$$

$$\begin{aligned} Cos\ t_{Sch}(t,s) = {} & Cos\ t_{El-N}(t,s) + Cos\ t_{Th-N}(t,s) + Cos\ t_{G-N} + Cos\ t_{PV}(t,s) \\ & + Cos\ t_{Wr}(t,s) + Cos\ t_{CHP}(t,s) + Cos\ t_B(t,s) + Cos\ t_{Fc}(t,s) \\ & + Cos\ t_{Th-S}(t,s) + Cos\ t_{C-S}(t,s) + Cos\ t_{El-DR}(t,s) \\ & + Cos\ t_{TH-DR}(t,s) + Cos\ t_{C-DR}(t,s) \end{aligned} \tag{40}$$

$$\cos T_{RE}(\mathrm{t,s}) = \cos T_{UN-EN}(\mathrm{t,s}) + \cos T_{CHP-EM}(\mathrm{t,s}) + \cos t_{fc-em}(\mathrm{t,s}) \tag{41}$$

$$\cos T_R\ (\mathrm{t,s}) = \left(VAR + \frac{1}{1-\alpha}\sum_{S=1}^{10} P_S \lambda_S\right) \tag{42}$$

The equations specify the cost of operating Fuel Cell Power Plants (FCPPs), Renewable Energy Sources (RESs), and devices for storing thermal/cooling energy. This cost includes factors such as electric energy production, hydrogen production, and hydrogen pumping [5]:

$$\begin{aligned} \cos t_{fc}(\mathrm{t,s}) = {} & \frac{1}{\eta f_c} \times \left(\Psi_g \times \left[p_{fs-el}(t,s) + P_{FC}^{CH}(T,S)\right] + \Psi_{H_2-PUMP}\right. \\ & \left. \times \left[P_{FC-EL}(t,s) \times \eta_{H_2}\right]\right) \end{aligned} \tag{43}$$

$$\cos t_{res}(\mathrm{t,s}) = \Psi_{wt} \times p_{wt}(\mathrm{t,s}) + \Psi_{pv} \times p_{pv}(\mathrm{t,s}) \tag{44}$$

$$\cos t_{th-s}(\mathrm{t,s}) = \Psi_{th-s} \times \left[p_{th-s}^{ch}(t,s) + p_{th-s}^{disch}(t,s)\right] \tag{45}$$

$$\cos t_{c-s}(t,s) = \Psi_{c-s} \times \left[p_{c-s}^{ch}(t,s) = p_{c-s}^{disch}(t,s)\right] \tag{46}$$

$$\cos t_{el-dr}(t,s) = \Psi_{el-p} \times \left[p_{el}^{shift,down}(t,s) + p_{em}^{shift,up}(t,s)\right] \tag{47}$$

$$\cos \mathrm{t_{c-dr}}(t,s) = \Psi_{c-dr} \times \left[p_c^{shift,downt}(t,s) + p_c^{shift,up}(t,s)\right] \tag{48}$$

PCHP(t,s)+η × PB(t,s)- PChiller- Ab (t,s) (49).

The equation represents the cost of purchasing electricity, heating, and gas from external networks. This cost is determined by the prices associated with each energy source:

$$\cos t_{el-n}(t,s) = \Psi_{el} \times p_{el-n}(t,s) \tag{50}$$

$$\cos t_{th-n}(\mathrm{t,s}) = \Psi_{th} \times p_{th-n}(t,s) \tag{51}$$

$$\text{cost } \mathrm{t_{g-n}}(t,s) = \Psi_g \times \left[p_g(t,s) + p_{chp}(t,s) + p_b(t,s)\right] \tag{52}$$

The equation computes the cost of emissions related to the upstream network and the Combined Heat and Power (CHP) system, steam boiler, and FPP (Fuel Power Plant) based on the emission factors of CO2, NO2, and SO2. The formula is used to determine the financial impact of these emissions on the overall cost:

$$\cos t_{un-em}(t,s)=[\Psi_{co2}\times em_{el-co2}(t,s)+\Psi_{nox}\times em_{el-no_x}(t,s)+\Psi_{so_2}\times em_{el-so_2}(t,s)]\times p_{el-n}(t,s) \tag{53}$$

$$\cos \mathrm{t_{chp\text{-}em}}(t,s)=\left[\Psi_{co2}\times em_{chp-co2}(t,s)+\Psi_{nox}\times em_{chp-no_x}(t,s)+\Psi_{so_2}\times em_{chp-so_2}(t,s)\right]\times p_{chp}(t,s) \tag{54}$$

$$\cos t_{b-em}(t,s)=[\Psi_{co2}\times em_{b-co2}(t,s)+\Psi_{nox}\times em_{b-no_x}(t,s)+\Psi_{so_2}\times em_{b-so_2}(t,s)]\times p_{b}(t,s) \tag{55}$$

$$\cos \mathrm{t_{fc\text{-}em}}(t,s)=[\Psi_{co2}\times em_{fc-co2}(t,s)+\Psi_{nox}\times em_{fc-no_x}(t,s)+\Psi_{so_2}\times em_{fc-so_2}(t,s)]\times p_{fc-el}(t,s) \tag{56}$$

2-. 11Power balance

The power balance in the proposed EH model is achieved through various energy producers to meet the demand for electricity, heating, and cooling. Equations 57–59 express the constraints for power balance in electricity, thermal energy, and cooling energy. The electricity requirement is fulfilled through the power generated by the WT and PV plants, with the EH interacting with the electricity market as needed. Thermal power generated by the boiler, CHP system, and FCPP, along with the thermal storage system's charging and discharging operations, are harnessed to cover the EH's thermal power needs and satisfy its thermal energy demand. A thermal DR program is employed to modify the thermal load and aid in meeting the thermal demand. Cooling needs are addressed by the cooling produced by electric/absorption chillers, the cooling storage system's charging and discharging processes, and the inclusion of the DR cooling program, as outlined in Equation (60). Electricity consumed by the CHP gas, steam boiler, FCPP, and the EH's gas demand is directly drawn from the relevant network, while the gas is sourced from the respective supply network [40]:

$$p_{el(t,s)=\eta_{tr}}\times p_{el-n}(t,s)+p_{wt}^{out}(t,s)+p_{wt}^{out}(t,s)+\eta_{chp_{el}}\times p_{chp}(t,s)_{p_{chiller_{el}}(t,s)}+\left[p_{cfc_{el}}(t,s)+p_{fc}^{disch}(t,s)\right]+\left[p_{pev}^{disch}(t,s)-p_{pev}^{ch}(t,s)\right]+\left[p_{el}^{shift,down}(t,s)-p_{el}^{shift,up}(t,s)\right] \tag{57}$$

$$p_{el(t,s)=}\mathrm{p_{th\text{-}n}(t,s)}+\eta_{\mathrm{chp_{th}}}\times \mathrm{p_{chp}(t,s)}+\eta_{\mathrm{b}}\times \mathrm{p_{b}(t,s)_{p_{chiller_{ab}}(t,s)}}+\mathrm{p_{fc_{th}}(t,s)}+\left[\mathrm{p_{th_s}^{disch}(t,s)_{p_{th_s}^{ch}(t,s)}}\right]+\left[p_{th}^{shift,down}(t,s)+p_{th}^{shift,up}(t,s)\right] \tag{58}$$

$$p_{c(t,s)=\eta_{chiller\_el}}\times p_{chiller\_el}(t,s)+\eta_{chiller_{ab}}\times p_{chp}(t,s)_{p_{chiller_{el}}(t,s)}+\left[p_{c_s}^{disch}(t,s)+p_{c_s}^{ch}(t,s)\right]+\left[p_{c}^{shift,down}(t,s)-p_{c}^{shift,up}(t,s)\right] \tag{59}$$

$$p_{g-n}(t,s)=p_{g}(t,s)+p_{chp}(t,s)+p_{b}(t,s)+\frac{p_{fc\_el}(t,s)+p_{fc}^{disch}}{\eta_{fc}(t,s)} \tag{60}$$

2-12. Grid and converter constraints

The limitations on electricity buying/selling in the electricity market are expressed in Equation (61). These constraints account for the minimum and maximum capacity of electrical grid infrastructure, including transmission lines and upstream transformers. Moreover, the desired level of hot water in the proposed SEH (Smart Energy Hub) is regulated by managing the quantity of thermal power bought or sold in the thermal market. Moreover, the import of gas power from the gas network is limited based on Equation (64), which considers factors such as the characteristics of gas network components (e.g., pipe diameter, friction coefficient). This equation also incorporates restrictions associated with the nominal capacity of the boiler, transformer, Combined Heat and Power (CHP) system, and electric and absorption chillers:

$$p_{el-n}^{min}(t,s)\le p_{el-n}(t,s)\le p_{el-n}^{max}(t,s) \tag{61}$$

$$p_{th-n}^{min}(t,s)\le p_{th-n}(t,s)\le p_{th-n}^{max}(t,s) \tag{62}$$

$$p_{g-n}^{min}(t,s)\le p_{g-n}(t,s)\le p_{g-n}^{max}(t,s) \tag{63}$$

$$\eta_{b}\times p_{b}(t,s)\le p_{b}^{cap} \tag{64}$$

$$\eta_{tr}\times p_{el-n}(t,s)\le p_{tr}^{cap} \tag{65}$$

$$\eta_{chp}\times p_{chp}(t,s)\le p_{chp}^{cap} \tag{66}$$

$$\eta_{chiller-el}\times p_{chiller-el}(t,s)\le p_{chiller-el}^{cap} \tag{67}$$

$$\eta_{chiller-ab}\times p_{chiller-ab}(t,s)\le p_{chiller-ab}^{cap} \tag{68}$$

2-13. Uncertainty model

To account for the uncertainty in demand and price, the forecast error distribution curves are divided into time intervals, each spanning one standard deviation. The deterministic approach uses the demand and price values as inputs for the uncertain model. The variance of demand and price is assumed to be 10 % on average. Fig. 2 illustrates a discrete representation of the probability distribution function for prediction errors. For each scenario, two quantities need to be calculated: the scenario's probability, determined by integrating the area under the probability distribution curve within each interval, and the average value of each interval representing the predicted error in that specific scenario. Table 2 presents the values and probabilities associated with each scenario.

To address the computational challenges posed by large scenario trees in stochastic optimization, it is crucial to reduce the number of scenarios. In this paper, the widely adopted approach of using the Kantorovich distance, denoted as $D_k(.)$, is employed. This distance metric allows for measuring the difference between two probability distributions, Q and Q′, as defined in the equation. By leveraging the Kantorovich distance, the scenario set can be effectively reduced, enabling more efficient and feasible optimization in the model [41]:

$$D_K(\mathrm{Q},\mathrm{Q}')-inf_{\eta}\left\{\int_{\Omega*\Omega}c(s,s')\eta(ds,ds'):\int_{\Omega}\eta(0,ds')-Q,\int_{\Omega}\eta(ds,0)-Q\right\} \tag{69}$$

$$\mathrm{c(s,s')}=\|s-s'\|^{T} \tag{70}$$

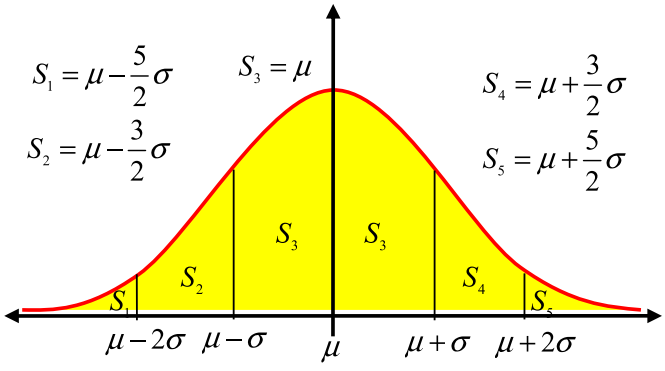

Fig. 2. Probability distribution function for uncertainty parameters.

Table 2
Probability of scenarios according to the normal distribution function.

Scenario number	value in each scenario	Probability in each scenario
S_1	$\mu - 2.5\sigma$	0.023
S_2	$\mu - 1.5\sigma$	0.136
S_3	μ	0.682
S_4	$\mu - 1.5\sigma$	0.136
S_5	$\mu - 2.5\sigma$	0.23

where the cost function $c(s, s')$ is non-negative, alternating, symmetric.

3. Proposed algorithm

The Slime Mold Algorithm (SMA) is an innovative metaheuristic algorithm inspired by the dynamic behavior of slime molds in nature. This algorithm includes distinctive features and a mathematical model that employs adaptive weights based on bio-oscillators to optimize the path-finding process for resource discovery, showcasing exceptional exploration abilities [42]. In comparison to other analogous metaheuristic algorithms such as GA and PSO, SMA demonstrates quicker convergence and attains optimal solutions in less computational time. The subsequent section offers insights into the mathematical principles underpinning this algorithm.

3-1. Mathematical model of SMA

Slime molds navigate towards food sources by following airborne chemical signals. To express this behavior mathematically, the following formulas are presented:

$$\overrightarrow{X}(t+1) = \begin{cases} \overrightarrow{X_b}(t) + \overrightarrow{vb}.\left(\overrightarrow{W}.\overrightarrow{X_A}(t) - \overrightarrow{X_B}(t)\right), r < p \\ \overrightarrow{vc}.\overrightarrow{X}(t), r \geq p \end{cases} \quad (71)$$

In this context, the parameter vb varies between -a and a, while the vector vc linearly decreases from one to zero. The variable t represents the current iteration, X_b represents the location with the highest odor concentration at the moment, and X represents the current location of the slime mold. X_A and X_B denote randomly selected values of the slime mold, and W signifies the weight of the slime mold. Furthermore, the relationship for p is computed as follows:

$$p = \tanh|S(i) - DF| \quad (72)$$

where $i \in 1, 2, \ldots, n$ and S(i) is the fitness coefficient of X. DF represents the best response obtained across all iterations [42]. The function range for vb and the relationship between a and W are as follows:

$$\overrightarrow{vb} = [-a, a] \quad (73)$$

$$a = \operatorname{arctan} h\left(-\left(\frac{t}{\max\_t}\right)+1\right) \quad (74)$$

$$\overrightarrow{W(SmellIndex)} = \begin{cases} 1 + r.\log\left(\frac{bF - S(i)}{bF - wF}\right)+1), condition \\ 1 - r.\log\left(\frac{bF - S(i)}{bF - wF}\right)+1), others \end{cases} \quad (75)$$

$$SmellIndex = sort(S) \quad (76)$$

In this context, the condition illustrates that S(i) holds primary significance within the population. Here, r represents a random value within the interval [0,1], bF signifies the optimal coefficient attained during the current iteration process, wF denotes the worst value acquired during the current iteration process, and SmellIndex represents the values sorted according to the best response. One of the pioneering approaches for tackling intricate issues involving nonlinear functions is the incorporation of chaotic search methods into intelligent algorithms, with the objective of enhancing their capabilities. Chaotic methods, rooted in nonlinear and nonconvex functions, have garnered substantial attention in recent times. The proposed chaotic method for problem-solving can be represented by the following relationship:

$$c_{i+1}^j = \begin{cases} 2c_i^j, if 0 < c_i^j \leq 0.5 \\ 2\left(1 - c_i^j\right), if 0.5 < c_i^j \leq 1 \end{cases}, j = 1, 2, \ldots, Ng, \{Tend\} \quad (77)$$

4. Simulation results and numerical analysis

The energy hub modeling in this article was conducted using MATLAB software, specifically the 2018 version. The modeling process took place on a personal computer with the following specifications: a 5 GB Intel processor, 512 GB storage capacity, and 6 MB cache.

4-1Case study

The information regarding PV, WT, FCPP, storage devices, green gas emission, energy networks, and the cost of demand resources can be found in Tables 3–9, respectively. Furthermore, Table 9 presents the predicted data for wind speed, solar radiation, atmospheric temperature, and the prices of electricity, heat, and gas networks. The deviation of PEV mileage was estimated to be 14 % of its expected value. The energy demands are modeled based on the expected values depicted in Fig. 3.

4.2. Results and analysis

In this section, we present the results and analysis of the conducted study. The obtained data from the simulations are analyzed to gain insights into the performance and effectiveness of the proposed approach.

Case 1. EH Base System - This case examines the system without the inclusion of PEVs, HSS, or DRP.

Case 2. EH with PEVs, HSS, and DRP - In this case, PEVs, HSS, and DRP are integrated into the system.

Case 3. EH with PEVs, HSS - Here, PEVs and HSS are implemented without DRP.

Case 4. EH with PEVs, HSS, and DRP - This case demonstrates the improved performance of the system through the utilization of PEVs, HSS, and DRP, harnessing the benefits of these technologies and programs.

To perform a probabilistic analysis of the proposed EH, a recommended simulation method is employed to generate numerous scenarios that consider uncertainties in variables like wind and solar generation. These scenarios are subsequently organized into 10 clusters. Fig. 4 illustrates the electricity market power transactions for the four case studies. It is evident that during off-peak hours, especially in the morning when electricity prices are low, the system procures electricity from the market in all scenarios. However, during peak hours (afternoon) when electricity prices are high, the system's reliance on purchasing electricity diminishes.

Table 3
Parameters of PV/WT plant [43].

Symbol	Amount	Symbol	Amount
P_{WT}^r	$400kW$	S^{std}	$1kW/m^2$
$W^{cut,in}$, W^r, $W^{cut,out}$	$4, 10, 22m/s$	C_T	$-0.00043C^\circ - 1$
A	0.0311	T^{std}	$25C^\circ$
B	−0.0776	η_{PV}^{con}	0.9
C	0.0174	$NOCT$	$45.5C^\circ$
η_{WT}^{con}	0.9	Ψ_{WT}	$0Cent/kWh$
N_{PV}^{pa}, N_{PV}^{se}	60, 80	Ψ_{PV}	$0Cent/kWh$

Table 4
Parameters of FCPP [44].

Symbol	Amount	Symbol	Amount
P_{FC}^{min}, P_{FC}^{max}	$0, 250kW$	η_{H_2}	0.95
$P_{FC}^{ch,min}$, $P_{FC}^{ch,max}$	$0, 500kW$	Ψ_{H_2-Pump}	$1Cent/kWh$

Table 5
Parameters of PEVs and storage devices [5,43].

Symbol	Amount	Symbol	Amount
η_{PEV}^{ch}, η_{PEV}^{disch}	0.9, 0.93	η_{Th-S}^{ch}, η_{Th-S}^{disch}	0.9, 0.9
ν	10	α_{Th-S}^{loss}, α_{C-S}^{loss}	0.02, 0.02
SOC^{min}, SOC^{max}	$1, 25kW$	P_{Th-S}^{cap}, P_{C-S}^{osscap}	$200, 200kW$
$P_{PEV}^{ch,min}$, $P_{PEV}^{ch,max}$	$0, 12.5kW$	φ_{C-S}^{min}, φ_{C-S}^{max}	0.05, 0.9
$P_{PEV}^{disch,min}$, $P_{PEV}^{disch,max}$	$0, 12.5kW$	η_{C-S}^{ch}, η_{C-S}^{disch}	0.9, 0.9
φ_{Th-S}^{min}, φ_{Th-S}^{max}	0.05, 0.9	Ψ_{Th-S}, Ψ_{C-S}	$2, 2Cent/kWh$

Table 6
Parameters of thermal and cooling convertors [43].

Symbol	Amount	Symbol	Amount
η_{CHP-EL}, η_{CHP-TH}	0.4, 0.35	P_{CHP}^{cap}	$800kW$
$\eta_{Chiller-El}$, $\eta_{Chiller-Ab}$	0.9, 0.85	P_{B}^{cap}	$800kW$
$P_{Chiller-El}^{cap}$, $P_{Chiller-Ab}^{cap}$	$800, 800kW$	η_{B}	0.85

Table 7
Parameters of green gas emissions [44].

Symbol	Amount
$Em_{El-CO_2}, Em_{El-NO_x}, Em_{El-SO_2}$	$0.723, 0.000199, 0.0000036kg/kWh$
$Em_{CHP-CO_2}, Em_{CHP-NO_x}, Em_{CHP-SO_2}$	$0.723, 0.000199, 0.0000036kg/kWh$
$Em_{B-CO_2}, Em_{B-NO_x}, Em_{B-SO_2}$	$0.502, 0.0005216, 0.00736kg/kWh$
$Em_{FC-CO_2}, Em_{FC-NO_x}, Em_{FC-SO_2}$	$0.921, 0.002295, 0.003583kg/kWh$
$\Psi_{CO_2}, \Psi_{NO_x}, \Psi_{SO_2}$	$0.014, 4.2, 0.99Cent/kg$

Table 8
Network and DR parameters [43].

Symbol	Amount
η_{Tr}	0.9
P_{Tr}^{cap}	$3000kW$
P_{EL-N}^{min}, P_{EL-N}^{max}	$-2000, 3000kW$
P_{Th-N}^{min}, P_{Th-N}^{max}	$-1000, 1000kW$
P_{G-N}^{min}, P_{G-N}^{max}	$0, 3500kW$
$\Psi_{El-Dr}, \Psi_{Th-Dr}, \Psi_{C-Dr}$	$2Cent/kWh$

When comparing case 1 to the remaining three cases, several noteworthy observations can be made. Firstly, during the time intervals spanning from 03:00 to 08:00, the PEVs in all cases are charged due to the availability of low electricity market prices. Conversely, between 19:00 and 22:00, the PEVs are discharged to sell surplus power back to the electricity market, aiming to minimize overall operational costs. In case 3, there is a higher demand for electric power between 01:00 and 04:00, as well as between 04:00 and 07:00, compared to the other cases. This increased demand is attributed to hydrogen production by the FC. Additionally, between 17:00 and 22:00, case 3 experiences a higher selling power due to the electricity generation by the FCPP and the discharge of hydrogen storage. During peak hours, typically occurring during the day, there is a significant trend across all cases to sell electricity. However, case 4 outperforms the other cases due to its greater flexibility. In case 4, there is a higher demand for electricity during the early hours of the day, primarily driven by the PEVs, FCPP, and DRP. Conversely, during the late hours of the day, case 4 demonstrates a higher level of electricity sales compared to the other cases. Overall, the results indicate that case 4, with the integration of PEVs, HSS, and DRP, exhibits a more efficient and dynamic operation with optimized electricity purchases and sales throughout the day.

Fig. 5 illustrates the thermal network's buying/selling activity. The graph provides a clear representation of the energy hub's behavior during the early morning period (01:00 to 07:00), where it sells thermal electricity to the market in response to favorable electricity and gas prices. During this time, the energy hub relies solely on the boiler and CHP to meet its heat requirements, as the gas price is lower than that of the thermal market. However, as we transition into the mid-morning hours (07:00 to 12:00), there is a gradual increase in the price of gas, leading the system to source its thermal requirements from the thermal market. During this period, the production of heat by the boiler and CHP becomes more expensive, primarily due to the suboptimal efficiency of the heat exchangers. Between 11:00 and 24:00, the gas price slightly decreases, encouraging a greater inclination to produce heat using the boiler and CHP. From 11:00 to 17:00, the energy hub sells thermal electricity to the market, while from 17:00 to 22:00, the thermal requirements are met by leveraging the thermal market. In case 4, there is an increased reliance on purchasing thermal power from the market later in the day, as it involves selling a greater amount of thermal power during specific hours. Fig. 6 presents the gas power obtained from the gas network. Notably, during the hours from 07:00 to 11:00, gas demand decreases since, as indicated in Fig. 5, the heat demand is met by the gas network during this timeframe. Between 07:00 and 11:00, the thermal production from the steam boiler decreases due to its inefficiency and the elevated gas prices. In contrast, from 18:00 until the end of the day, the gas consumption of the steam boiler decreases while the CHP system operates at maximum capacity. This is because the higher electricity market prices during these hours make electricity generation through the CHP system more advantageous.

Fig. 7 illustrates the thermal power, electrical power, and the charging/discharging status of the Fuel Cell Power Plants (FCPP). Cases 1 and 2 are not included in this figure as they do not involve fuel cells. The electric power generated by the fuel cells in cases 3 and 4 is represented by the blue and black curves, respectively. During the evening hours (after 17:00) when electricity prices are high, there is a tendency to prioritize the utilization of gas in the Fuel Cell Power Plant (FCPP) for electricity generation. The FCPP is also active during the early hours of the day. The thermal output of the fuel cells in cases 3 and 4, represented by the red and green curves, corresponds to the fluctuations in gas and electricity prices in the market. Thermal generation occurs simultaneously with electricity generation. The charging of the tank takes place during the early hours, and its discharge occurs during the later hours of the day. This pattern remains consistent across all cases. Plug-in Electric Vehicles (PEVs) are charged during the periods of low electricity prices in the early hours of the day. Conversely, they can be discharged during the peak hours of the day when electricity prices are higher in the market.

The thermal generation of fuel cells corresponds to electricity generation. Furthermore, the charging of the tank occurs in the early hours of the day, while discharging takes place during the later hours. PEVs are charged during the periods of low electricity prices in the early hours, while they can be discharged during the peak hours when electricity prices are high in the market. This behavior remains consistent across all cases. This figure provides valuable insights into the relationship between electricity prices, fuel cell thermal output, and the charging/discharging patterns of PEVs. It highlights the dynamic nature of energy management and the optimization strategies employed to maximize energy utilization and cost efficiency throughout the day.

Fig. 8 depicts the charging and discharging statuses of the PEVs. The graph provides a clear depiction of the PEVs' behavior, showing that they are in the charging state during the early hours of the day when electricity market prices are low. However, during the peak hours of the day when electricity prices in the market are high, the PEVs have the ability to discharge their stored energy. This behavior remains consistent across all cases, highlighting a uniform pattern across various scenarios.

Table 9
Historical records of wind speed, solar radiation, atmospheric temperature, and prices of electricity, heat, and gas networks [5,44].

Hour	Wind speed (W/m^2)	Solar radiation (W/m^2)	Atmospheric temperature	Electric Network price (cent/kWh)	Thermal Network price (cent/kWh)	Gas Network price (cent/kWh)
1	14.00	0	13.70	5	10.25	5.00
2	14.30	0	13.50	5	9.95	5.00
3	13.65	0	9.60	5	10.25	5.00
4	13.85	0	10.10	3	10.4	5.625
5	15.65	0	10.8	3	10.45	6.25
6	9.70	19.00	7.85	3	10.2	6.25
7	9.50	47.50	7.85	5	6.85	6.25
8	9.40	190.00	9.6	7	7.35	6.25
9	9.45	503.50	13.90	7	6.85	6.25
10	9.50	665.00	16.65	7	6.4	6.25
11	8.10	807.50	19.40	9	6.80	6.87
12	11.9	902.50	22.00	10	9.75	7.50
13	12.8	760.00	26.45	10	10.34	7.50
14	11.7	380.00	28.40	11	10.4	7.50
15	10.3	399.00	27.95	11	9.82	6.87
16	8.30	665.00	26.00	11	9.3	6.25
1	8.40	570.00	26.00	11	10.90	6.25
18	6.10	361.00	26.45	13	8.00	6.25
9	5.65	228.00	26.95	14	7.75	6.25
20	7.6	38.00	24.50	17	7.85	6.25
21	9.70	19.00	24.30	17	7.75	6.25
22	5.95	0	20.60	17	7.65	5.62
23	2	0	21.55	10	8.00	5.00
24	2.45	0	15.70	7	8.30	5.00

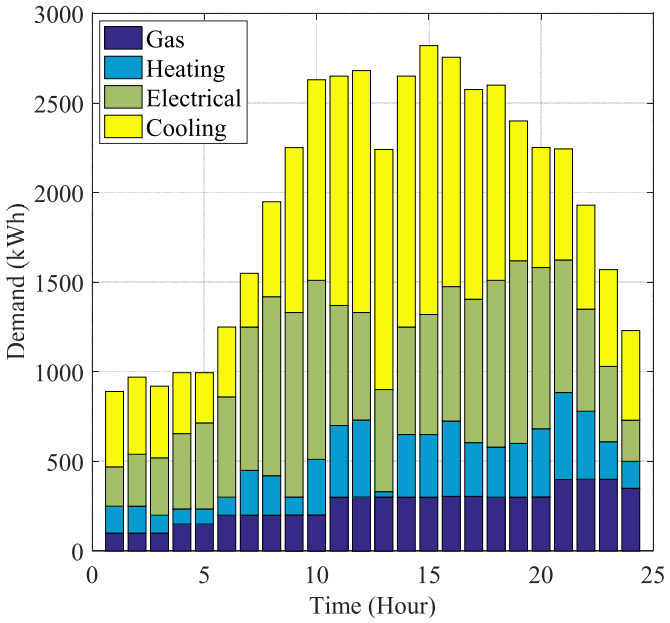

Fig. 3. Energy demands [44].

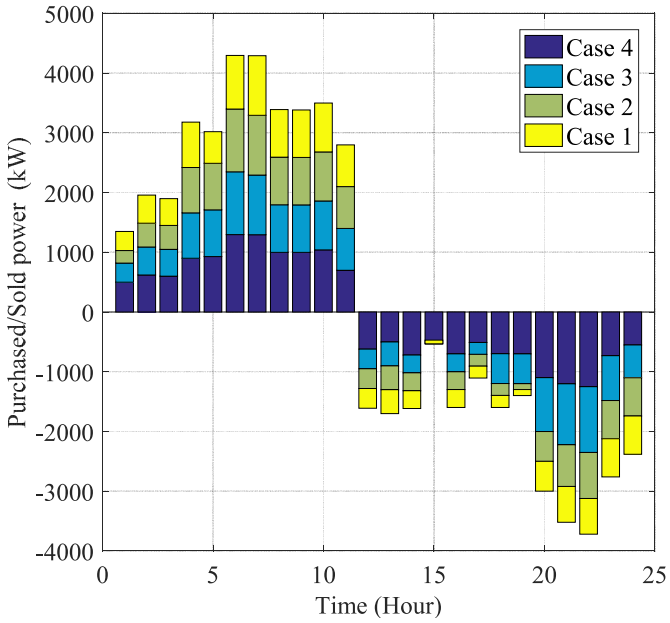

Fig. 4. Illustrates the power purchased/sold from/to the electricity market.

Fig. 9 displays the power of the heat storage system for charging and discharging. It is apparent that during the time period between 6 and 8, characterized by low thermal market prices and sufficient fulfillment of thermal demand by other heat-generating devices, the heat storage system is charged to store energy for future utilization. Conversely, from 16 to 19, the stored heat is discharged to meet the thermal needs of the system. This behavior is consistent across all cases, indicating a similar pattern.

Fig. 10 illustrates the charging and discharging of the cooling storage system, influenced by the electricity market, heat market, and gas market. The charging of the cooling storage system occurs between 05:00 and 07:00, coinciding with a period of lower electricity market prices, making it advantageous for charging. From 13:00 to 19:00, the cooling storage system is discharged to meet the cooling requirements of the energy hub. During this time, the use of chillers is more pronounced, resulting in higher electricity prices for the energy hub. The cooling storage system is employed to mitigate these costs. Between 13 and 15, there is a change in cooling demand, and the demand response schedule is low. As a result, the electric chiller consumes less electricity during this hour compared to others. Consequently, the cooling storage system is depleted to meet the increased cooling demand. From 16 to 17, the discharge of the cooling storage system is reduced. There are two reasons for this: Firstly, the cooling storage absorbs a portion of the cooling load, and at other times, it employs demand response programming for cooling purposes. Secondly, the upper part of the system utilizes chillers to meet the cooling demand. Between 18:00 and 19:00, the cooling storage experiences a greater depletion, as the contribution from chillers (both electric and absorption) is reduced during this time interval.

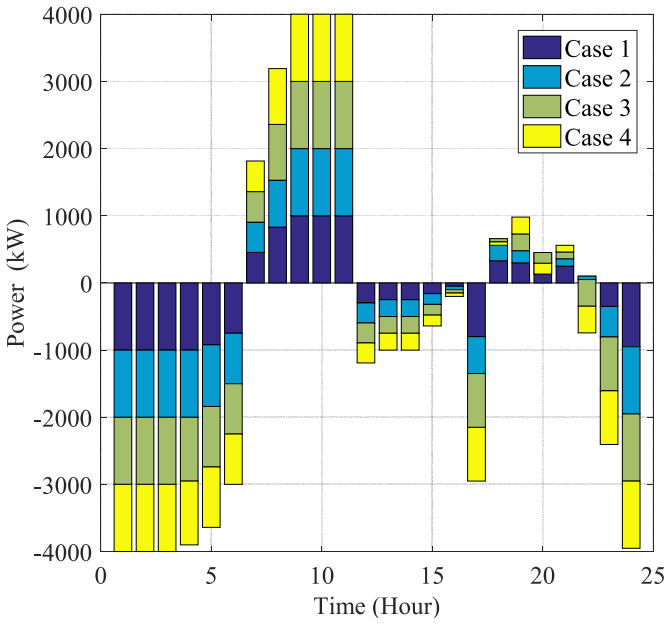

Fig. 5. Illustrates the power bought/sold from/to the thermal network.

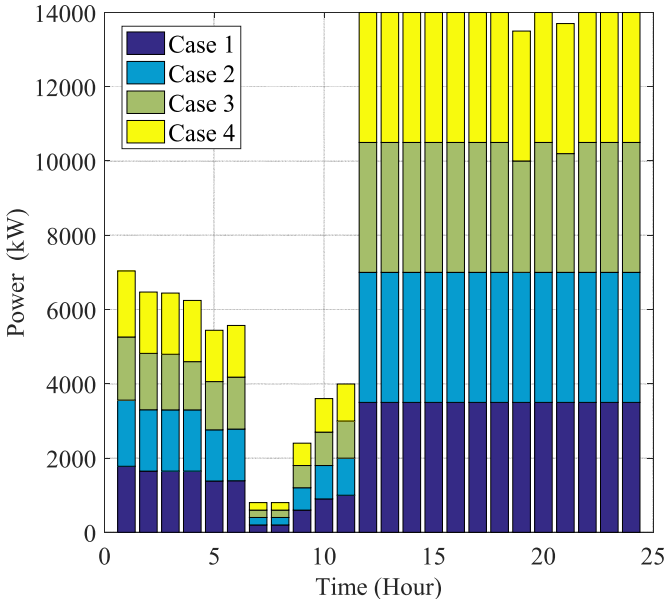

Fig. 6. Displays the purchased gas power from the gas network.

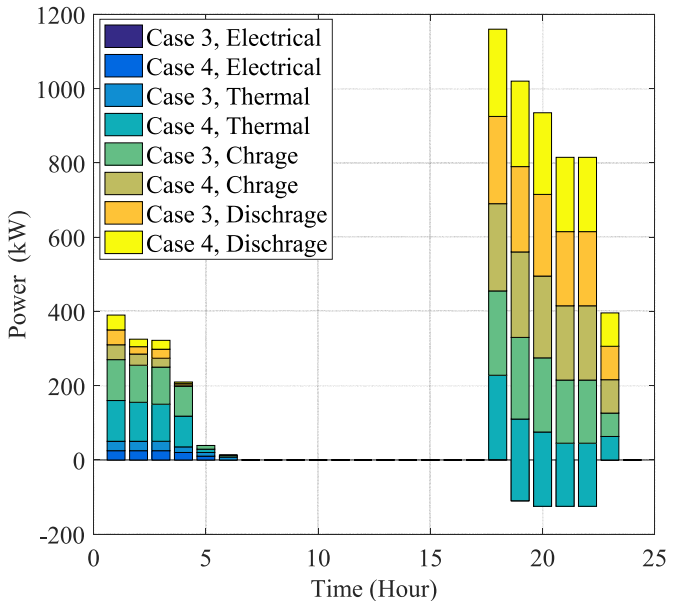

Fig. 7. FC Electrical/thermal power generation, electric power of the hydrogen production and consumption.

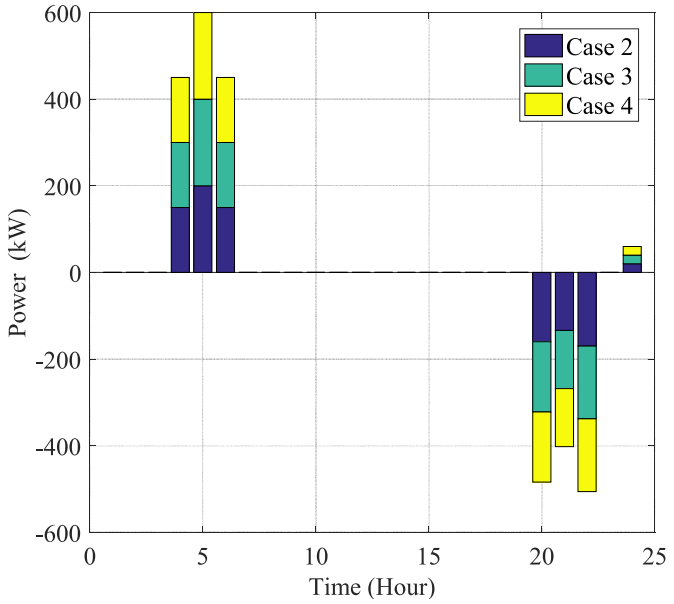

Fig. 8. Charge/discharge power of the PEVs.

Fig. 11 depicts the electrical and absorption power of chillers. During the early hours of the day (01:00–08:00), there is a demand for cooling, and customers utilize electric chillers due to the lower electricity prices. Subsequently, the absorption chiller comes into operation. From 07:00 to 11:00 and between 10:00 and 17:00, both electric and absorption chillers are active, with the absorption chiller dominating the output. During these periods, when heat and gas market prices are lower, the electric chiller is turned off between 19:00 and 24:00. The cooling demands are exclusively fulfilled by the absorption chiller during these hours, as its output capacity adequately meets the cooling requirements. In the fourth mode, the electric chiller consumes less electricity from 11:00 to 18:00, leading to higher electricity consumption between 01:00 and 09:00. Furthermore, in mode 4, the absorption chiller experiences an augmented supply of thermal power from 18:00 to 23:00. This adjustment is achieved by implementing cooling demand response programs that shift the cooling demand from the midday period to the morning, when electricity prices are lower, and to the late hours of the day, when gas and heat market prices are reduced.

Fig. 12 clearly demonstrates a redistribution of demand during peak hours with high electricity market prices, leading to a negative load shift. This shift indicates a diversion of demand away from those specific hours. For instance, hours 1 to 13 exhibit a demand shift to other periods due to the comparatively lower electricity market prices during that timeframe. The thermal demand response, depicted by the black curve, is influenced by gas prices. The thermal market prices rise in the early hours of the day due to lower gas prices in the market. Furthermore, the heat demand experiences downward shifts between 05:00 and 07:00 and 18:00 and 18:00, corresponding to high gas and heat market prices. Subsequently, the thermal market price decreases between 07:00 and 08:00, resulting in an upward shift in the thermal demand. The cooling demand undergoes fluctuations from the early afternoon until late in the

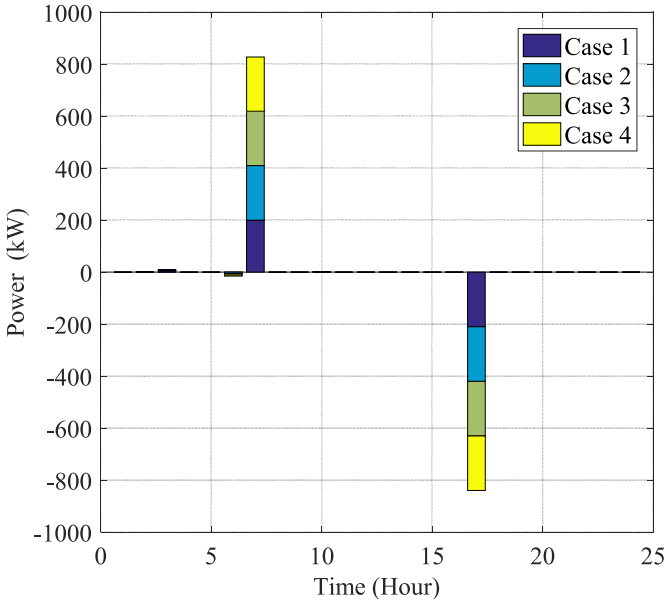

Fig. 9. Charge and discharge power of heat storage.

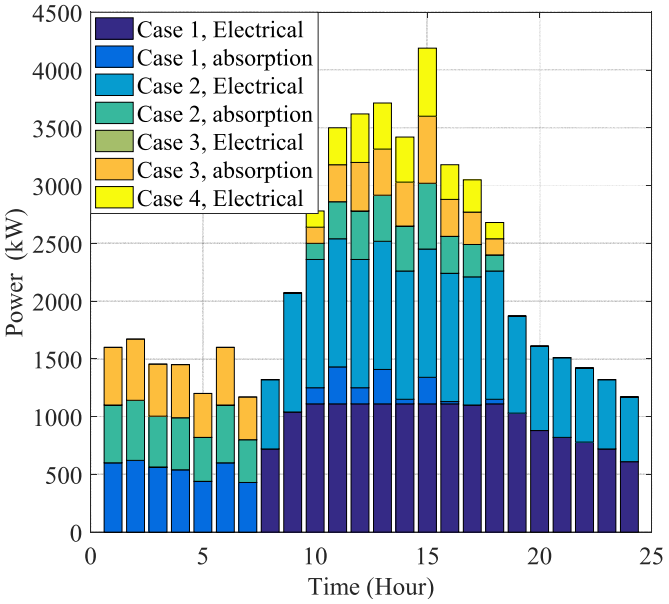

Fig. 11. Electrical/Absorption chiller power.

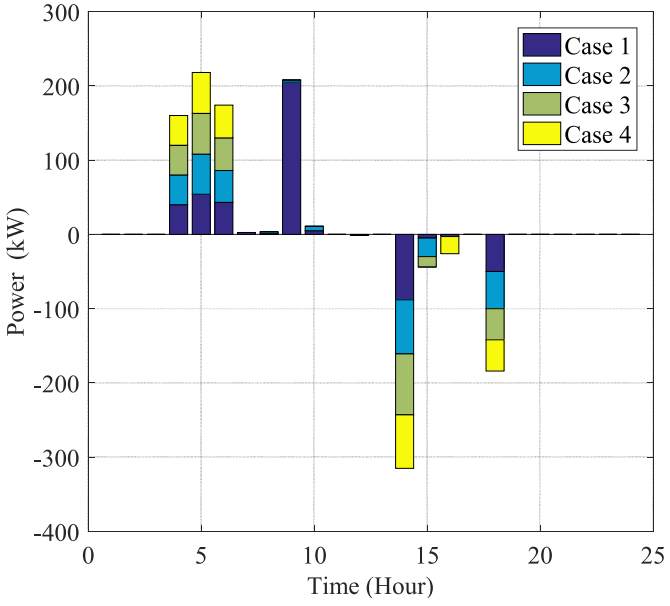

Fig. 10. Charge and discharge power of cooling storage.

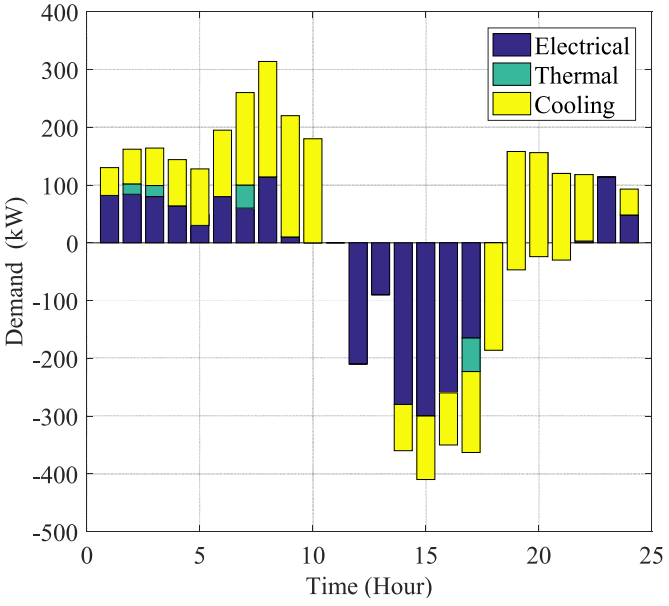

Fig. 12. Increased and decreased electrical, thermal and cooling load demands with DR programs.

day. Meeting the cooling demand becomes more expensive during midday when heat market prices are high. However, by leveraging the low electricity market prices during the early hours of the day, the cooling demand is shifted to that time period, taking advantage of the available electricity supply.

In the latter part of the day, the cooling demand can be effectively met by utilizing low-priced heat from the thermal market. It is noticeable that the thermal demand response program (thermal DRP) has a relatively smaller impact on the overall load compared to the electrical and cooling demand response programs (electrical and cooling DRPs). This difference arises from the fact that the thermal market prices remain relatively consistent across different time periods. Nevertheless, in the morning timeframe from 07:00 to 09:00, when the price of heat in the market is lower, the heat is stored and then discharged to meet the thermal needs of the system. This procedure limits the extent to which the thermal demand response program (thermal DRP) can affect the

Table 10
Simulation results for different case studies in the deterministic scheme.

	Case No.	Operation Cost Minimization	Emission Cost Minimization	Operation + Emission Minimization
Operation cost ($)	1	2465.43	3132.13	2443.21
	2	2419.18	3157.17	2401.28
	3	2301.25	3154.27	2301.45
	4	2199.32	3134.18	2199.32
Emission cost ($)	1	5.33	2.14	5.34
	2	5.54	2.18	5.37
	3	5.09	1.65	5.64
	4	4.45	0.76	4.65

Table 11
Simulation results for different case studies in the stochastic scheme.

	Case No	Operation Cost Minimization	Emission Cost Minimization	Risk Cost Minimization	Operation + Emission + Risk cost Minimization
Operation cost ($)	1	2712.15	3387.21	2909.54	2721.64
	2	2654.31	3389.43	2875.21	2712.32
	3	2524.02	3365.21	2732.97	2543.38
	4	2427.16	3312.43	2612.87	2508.12
Emission cost ($)	1	6.03	2.76	5.32	5.43
	2	6.12	2.67	5.27	5.46
	3	5.43	1.54	5.18	5.21
	4	5.17	1.43	5.23	5.16
Risk cost ($)	1	576.11	686.32	291.53	315.27
	2	556.09	702.43	265.32	309.11
	3	534.21	711.34	265.39	292.54
	4	511.65	738.36	262.21	283.09

system. Consequently, the impact of the thermal DRP on the efficiency of thermal elements, such as storage, and the interaction of thermal power with the thermal market is kept to a minimum.

In this section, we provide the simulation outcomes for both deterministic and random optimization strategies, showcased in Tables 10 and 11, respectively. Within the deterministic plan, three distinct objective functions are put forth. The initial two approaches center around enhancing the operation cost and emissions independently, whereas the third approach strives to concurrently minimize both aspects. In the first approach, the operation cost experiences reductions of 2 %, 7 %, and 11 % in the second, third, and fourth instances, respectively, in comparison to the first scenario. These findings effectively illustrate the economic advantages derived from the integration of various technologies. The second approach specifically targets the reduction of emission costs, resulting in a 16.89 % decrease in emission costs in the third case and a significant 65 % reduction in the fourth case. However, in the second case, there is a slight increase of 1 % in emission costs. In the third approach, where both operational and emission costs are concurrently minimized, an overall reduction in system costs is achieved. Specifically, in the second, third, and fourth scenarios, the operational cost decreases by 2.54 %, 7.32 %, and 12.65 %, respectively. Moreover, in the third and fourth cases, there are reductions of 6.67 % and 15.43 % in publication cost, respectively, while a slight increase of 1.34 % is observed in the second case. It is important to note that the results presented in the table summary for the second case are random in nature.

Fig. 13 displays the results of the risk analysis for different risk aversion parameters. The figure clearly demonstrates that increasing the values of the risk aversion parameter β leads to a decrease in the EH risk cost while simultaneously increasing the operation costs. On the other hand, opting for a more cost-effective solution with a higher level of risk can be achieved by using smaller values of β.

5. Conclusions and future work

In conclusion, this study explored the performance of a system that integrated Plug-in Electric Vehicles (PEVs), Heating Storage Systems (HSS), and Demand Response Programs (DRP) within an energy hub framework. Four distinct case studies were conducted to assess the system's operation under various configurations. The findings underscored the effectiveness of the proposed approach in optimizing energy utilization and enhancing cost efficiency. During off-peak hours, the system adeptly procured electricity from the market at favorable prices. In contrast, during peak hours, it curtailed electricity purchases, resulting in cost reductions. Case 4, which featured the integration of PEVs, HSS, and DRP, emerged as the most promising configuration. This setup facilitated dynamic operations, optimizing electricity transactions with the market, the utilization of the thermal network, gas power procurement, and electricity generation through Fuel Cell Power Plants. The charging and discharging status of PEVs and storage systems played a pivotal role in achieving overall efficiency. The simulation results, encompassing both deterministic and random optimization strategies, demonstrated substantial reductions in costs and emissions as a result of the proposed approach. The integration of PEVs, HSS, and DRP significantly improved the system's overall performance. These findings suggest that implementing the proposed approach in real-world energy systems has the potential to enhance energy management, reduce costs, and promote sustainability. Further research and practical

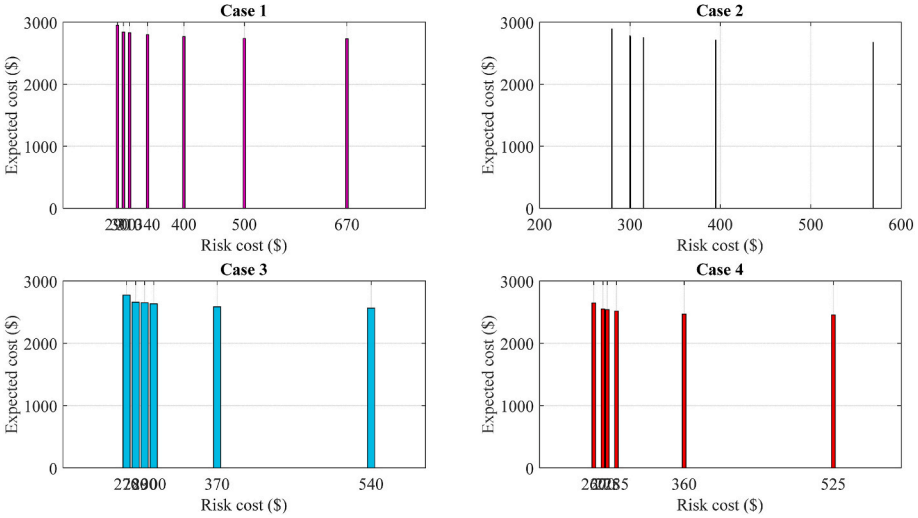

Fig. 13. The sensitivity of the operation/risk cost with regard to β variations.

implementation of this approach could contribute to the development of smart and efficient energy infrastructure. It is important to note that the study's conclusions are based on specific assumptions and parameters utilized in the simulations. Real-world implementations may necessitate additional considerations and adaptations to account for specific local conditions, regulations, and infrastructure. Nonetheless, the results offer valuable insights into the potential advantages of integrating PEVs, HSS, and DRP into energy hub systems. In the conducted study, the integration of Plug-in Electric Vehicles (PEVs), High-Performance Storage Systems (HSS), and Demand Response Programs (DRP) into the energy hub framework demonstrated remarkable cost reductions. Notably, Case 4, which encompassed all three technologies, displayed the most promising outcomes. It achieved a substantial 11 % reduction in operation costs, translating into a tangible operational cost of $2199.32. Simultaneously, this configuration realized an impressive 65 % reduction in emission costs, resulting in an emission cost of $0.76. When examining the deterministic scheme, the results revealed that the simultaneous minimization of operation and emission costs in Case 4 led to a 12.65 % decrease in overall operation costs, achieving a combined cost reduction of $266.11. Furthermore, this configuration enabled efficient risk management, with a notable 54 % reduction in risk costs, amounting to $262.21. It is worth noting that while Case 4 excelled in cost reduction, the other cases still exhibited noteworthy reductions in operational, emission, and risk costs, albeit to a slightly lesser extent. Transitioning to the stochastic scheme, Case 4 continued to demonstrate impressive outcomes. It achieved an 11 % reduction in operational costs, equivalent to an operational cost of $2427.16. Simultaneously, there was a 1.43 % reduction in emission costs, reaching an emission cost of $5.16. Additionally, risk management in Case 4 was robust, with a 47.6 % reduction in risk costs, amounting to $283.09. These numerical results not only underline the cost-efficiency of integrating PEVs, HSS, and DRP but also highlight the resilience and adaptability of Case 4 in managing operational, environmental, and risk-related aspects. Such tangible reductions in costs and emissions emphasize the real-world applicability and benefits of these integrated technologies for optimizing energy management systems.

For future work, focus on the development of smart grid technologies and infrastructure to enable seamless integration and optimal utilization of PEVs, HSS, and DRP. A smart grid incorporates advanced communication, monitoring, and control systems that enable real-time coordination and optimization of energy resources. By integrating PEVs, HSS, and DRP into the smart grid, it becomes possible to manage and balance the supply and demand of electricity effectively, maximize renewable energy utilization, and reduce grid stress during peak periods.

Funding

This work was supported by The National Social Science Fund of China (No.23BGL219), supported by the Social Science Foundation of Hubei Province (No. 21ZD081) and supported by The Key Project of Scientific Research Program of Hubei Education Department (No. D20191803).

CRediT authorship contribution statement

Chengying Yang: Writing - review & editing, Methodology, Algorithm design. **Zhixin Wu:** Investigation, Methodology, Supervision, Data curation, Writing - review & editing. **Xuetao Li:** Writing - review & editing, Writing - review & editing, Formal analysis. **Ashk Fars:** Preliminary preparation, Conceptualization.

Declaration of Competing interest

The authors declare that they have no known competing financial interests or personal relationships that could have appeared to influence the work reported in this paper.

Data availability

The authors do not have permission to share data.

References

[1] Tian H, Wang K, Cui X, Chen Z, Zhao E, Saeedi S. Multi-objective planning of microgrid based on renewable energy sources and energy storage system. J Energy Storage 2023;68:107803.
[2] Zhang T, Sobhani B. Optimal economic programming of an energy hub in the power system while taking into account the uncertainty of renewable resources, risk-taking and electric vehicles using a developed routing method. Energy 2023;271:126938.
[3] Abedinia O, Ghasemi-Marzbali A, Shafiei M, Sobhani B, Gharehpetian GB, Bagheri M. A multi-level model for hybrid short term wind forecasting based on SVM, wavelet transform and feature selection. In: 2022 IEEE international conference on environment and electrical engineering and 2022 IEEE industrial and commercial power systems europe (EEEIC/I&CPS europe). IEEE; 2022, June. p. 1–6.
[4] Huang S, Abedinia O. Investigation in economic analysis of microgrids based on renewable energy uncertainty and demand response in the electricity market. Energy 2021;225:120247.
[5] Allahvirdizadeh Y, Galvani S, Shayanfar H. Data clustering based probabilistic optimal scheduling of an energy hub considering risk-averse. Int J Electr Power Energy Syst 2021;128:106774.
[6] Li Q, Li Q, Wang C. Unit combination scheduling method considering system frequency dynamic constraints under high wind power share. Sustainability 2023;15(15):11840.
[7] Abedinia O, Lotfi M, Bagheri M, Sobhani B, Shafie-Khah M, Catalão JP. Improved EMD-based complex prediction model for wind power forecasting. IEEE Trans Sustain Energy 2020;11(4):2790–802.
[8] Tostado-Véliz M, Jordehi AR, Mansouri SA, Jurado F. A two-stage IGDT-stochastic model for optimal scheduling of energy communities with intelligent parking lots. Energy 2023;263:126018.
[9] Vonžudaitė O, Martišauskas L, Bakas R, Urbonienė S, Urbonas R. Optimization of heat pump systems in buildings by minimizing costs and CO2 emissions. Appl Sci 2023;13(8):4864.
[10] Papadimitriou C, Di Somma M, Charalambous C, Caliano M, Palladino V, Cortés Borray AF, Graditi G. A comprehensive review of the design and operation optimization of energy hubs and their interaction with the markets and external networks. Energies 2023;16(10):4018.
[11] Zhang X, Lovati M. Integration of urban energy systems with renewable envelope solutions at building cluster level. In: Future urban energy system for buildings: the pathway towards flexibility, resilience and optimization. Singapore: Springer Nature Singapore; 2023. p. 9–48.
[12] Guo Y, Zhou W, Ren H, Yu Y, Xu L, Fuss M. Optimizing the aluminum supply chain network subject to the uncertainty of carbon emissions trading market. Resour Pol 2023;80:103247.
[13] Yao R, Hu Y, Varga L. Applications of agent-based methods in multi-energy systems—a systematic literature review. Energies 2023;16(5):2456.
[14] Masihabadi D, Kalantar M, Majd Z, Saravi SVS. A novel information gap decision theory-based demand response scheduling for a smart residential community considering deep uncertainties. In: IET generation. Transmission & Distribution; 2023.
[15] Zhong J, Li Y, Wu Y, Cao Y, Li Z, Peng Y, et al. Optimal operation of energy hub: an integrated model combined distributionally robust optimization method with stackelberg game. IEEE Trans Sustain Energy 2023 July 2023;14(3):1835–48.
[16] Arumugham V, Ghanimi HM, Pustokhin DA, Pustokhina IV, Ponnam VS, Alharbi M, Sengan S. An artificial-intelligence-based renewable energy prediction program for demand-side management in smart grids. Sustainability 2023;15(6):5453.
[17] Liu H, Liu Q, Rao C, Wang F, Alsokhiry F, Shvetsov AV, Mohamed MA. An effective energy management Layout-Based reinforcement learning for household demand response in digital twin simulation. Sol Energy 2023;258:95–105.
[18] Akbari E, Shabestari SFM, Pirouzi S, Jadidoleslam M. Network flexibility regulation by renewable energy hubs using flexibility pricing-based energy management. Renew Energy 2023;206:295–308.
[19] Habib S, Aghakhani S, Nejati MG, Azimian M, Jia Y, Ahmed EM. Energy management of an intelligent parking lot equipped with hydrogen storage systems and renewable energy sources using the stochastic p-robust optimization approach. Energy 2023:127844.
[20] Lu Y, Yang L, Yang K, Gao Z, Zhou H, Meng F, Qi J. A distributionally robust optimization method for passenger flow control strategy and train scheduling on an urban rail transit line. Engineering 2022;12:202–20.
[21] Ke GY. Managing reliable emergency logistics for hazardous materials: a two-stage robust optimization approach. Comput Oper Res 2022;138:105557.
[22] Rangu SK, Lolla PR, Dhenuvakonda KR, Singh AR. Recent trends in power management strategies for optimal operation of distributed energy resources in microgrids: a comprehensive review. Int J Energy Res 2020;44(13):9889–911.
[23] Khalilabadi SMG, Zegordi SH, Nikbakhsh E. A multi-stage stochastic programming approach for supply chain risk mitigation via product substitution. Comput Ind Eng 2020;149:106786.
[24] Habib S, Aghakhani S, Nejati MG, Azimian M, Jia Y, Ahmed EM. Energy management of an intelligent parking lot equipped with hydrogen storage systems

and renewable energy sources using the stochastic p-robust optimization approach. Energy 2023:127844.
[25] Mirzapour-Kamanaj A, Majidi M, Zare K, Kazemzadeh R. Optimal strategic coordination of distribution networks and interconnected energy hubs: a linear multi-follower bi-level optimization model. Int J Electr Power Energy Syst 2020; 119:105925.
[26] Lu X, Liu Z, Ma L, Wang L, Zhou K, Yang S. A robust optimization approach for coordinated operation of multiple energy hubs. Energy 2020;197:117171.
[27] Hemmati M, Abapour M, Mohammadi-Ivatloo B, Anvari-Moghaddam A. Risk-based optimal operation of coordinated natural gas and reconfigurable electrical networks with integrated energy hubs. IET Renew Power Gener 2021;15(12): 2657–73.
[28] Pakdel MJV, Sohrabi F, Mohammadi-Ivatloo B. Multi-objective optimization of energy and water management in networked hubs considering transactive energy. J Clean Prod 2020;266:121936.
[29] Karkhaneh J, Allahvirdizadeh Y, Shayanfar H, Galvani S. Risk-constrained probabilistic optimal scheduling of FCPP-CHP based energy hub considering demand-side resources. Int J Hydrogen Energy 2020;45(33):16751–72.
[30] Fan L, Ji D, Lin G, Lin P, Liu L. Information gap-based multi-objective optimization of a virtual energy hub plant considering a developed demand response model. Energy 2023;276:127462.
[31] Shen B, Li M, Bohlooli N. Economic, environmental, and reliability assessment of distribution network with liquid carbon-based energy storage using multi-objective group teaching optimization algorithm. J Clean Prod 2023;404:136811.
[32] Mokaramian E, Shayeghi H, Sedaghati F, Safari A, Alhelou HH. A CVaR-Robust-based multi-objective optimization model for energy hub considering uncertainty and E-fuel energy storage in energy and reserve markets. IEEE Access 2021;9: 109447–64.
[33] Farsangi AS, Hadayeghparast S, Mehdinejad M, Shayanfar H. A novel stochastic energy management of a microgrid with various types of distributed energy resources in presence of demand response programs. Energy 2018;160:257–74.
[34] AbdelHady R. Modeling and simulation of a micro grid-connected solar PV system. Water Science 2017;31(1):1–10.
[35] Soroudi A, Keane A. Risk averse energy hub management considering plug-in electric vehicles using information gap decision theory. In: Plug in electric vehicles in smart grids. Energy Management; 2015. p. 107–27.
[36] Pazouki S, Haghifam MR. Optimal planning and scheduling of energy hub in presence of wind, storage and demand response under uncertainty. Int J Electr Power Energy Syst 2016;80:219–39.
[37] Mehrjerdi H, Hemmati R. Electric vehicle charging station with multilevel charging infrastructure and hybrid solar-battery-diesel generation incorporating comfort of drivers. J Energy Storage 2019;26:100924. .
[38] Wei P, He F, Li L, Shi X, Simoes R. Multi-objective problem based operation and emission cots for heat and power hub model through peak load management in large scale users. Energy Convers Manag 2018;171:411–26. .
[39] Jadidbonab M, Dolatabadi A, Mohammadi-Ivatloo B, Abapour M, Asadi S. Risk-constrained energy management of PV integrated smart energy hub in the presence of demand response program and compressed air energy storage. IET Renew Power Gener 2019;13(6):998–1008.
[40] Vahid-Pakdel MJ, Nojavan S, Mohammadi-Ivatloo B, Zare K. Stochastic optimization of energy hub operation with consideration of thermal energy market and demand response. Energy Convers Manag 2017;145:117–28.
[41] Li H, Ren Z, Fan M, Li W, Xu Y, Jiang Y, Xia W. A review of scenario analysis methods in planning and operation of modern power systems: methodologies, applications, and challenges. Elec Power Syst Res 2022;205:107722. .
[42] Nguyen TT, Wang HJ, Dao TK, Pan JS, Liu JH, Weng S. An improved slime mold algorithm and its application for optimal operation of cascade hydropower stations. IEEE Access 2020;8:226754–72.
[43] Rakipour D, Barati H. Probabilistic optimization in operation of energy hub with participation of renewable energy resources and demand response. Energy 2019; 173:384–99.
[44] Nazari-Heris M, Abapour S, Mohammadi-Ivatloo B. Optimal economic dispatch of FC-CHP based heat and power micro-grids. Appl Therm Eng 2017;114:756–69.